

NACA RM A56C08



Declassified by authority of NASA
Classification Change Notices No. 70
Dated ** 7/20/66

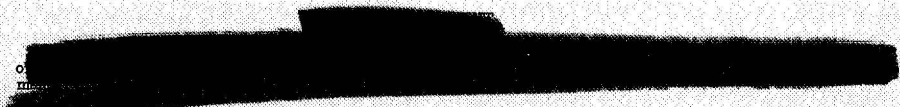
RESEARCH MEMORANDUM

A SUMMARY OF RESULTS OBTAINED DURING FLIGHT SIMULATION
OF SEVERAL AIRCRAFT PROTOTYPES WITH VARIABLE-
STABILITY AIRPLANES

By Walter E. McNeill and Brent Y. Creer

Ames Aeronautical Laboratory
Moffett Field, Calif.

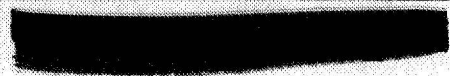
DECLASSIFIED- U S 1391
AUTHORITY- MEMO, DROBKA TO
LEBOW DATED. 6/30/66


NATIONAL ADVISORY COMMITTEE
FOR AERONAUTICS

WASHINGTON

May 25, 1956

60



NATIONAL ADVISORY COMMITTEE FOR AERONAUTICS

RESEARCH MEMORANDUMA SUMMARY OF RESULTS OBTAINED DURING FLIGHT SIMULATION
OF SEVERAL AIRCRAFT PROTOTYPES WITH VARIABLE-
STABILITY AIRPLANES

By Walter E. McNeill and Brent Y. Creer

SUMMARY

Two airplanes, an F6F-3 and an F-86A, each fitted with servo equipment for varying in flight the lateral and directional stability and handling characteristics, have been flown by test pilots of the aircraft industry and the NACA to simulate the predicted dynamic behavior of six prototype airplanes. During these simulation programs, flight experience was obtained with lateral oscillatory characteristics representative of those predicted for each prototype and with other unusual characteristics associated with certain specific designs. In cases where unusual characteristics were predicted, or where use of auxiliary damping devices was contemplated, the company test pilots gained familiarity with the trends in lateral behavior involved and were able to define ranges of acceptable characteristics which could be used as design criteria.

The methods of simulation and the types and ranges of variables considered are presented and the results of the individual programs are discussed. In addition, trends in pilot opinions of the lateral oscillatory characteristics are discussed in relation to current flying-qualities specifications.

INTRODUCTION

Design trends associated with recent increases in operational speeds and altitudes of military and research aircraft have resulted in dynamic stability and control characteristics which sometimes differ widely from those previously experienced in flight. Several criteria for satisfactory flying qualities have been developed as guides to aid airplane manufacturers in judging the suitability of their designs from the stability and control standpoint and as minimum requirements to be met by designers of military aircraft. The most recent of the military specifications for



flying qualities of piloted airplanes is presented in reference 1; other published criteria for the more limited case of lateral oscillatory characteristics are given in references 2, 3, 4, and 5.

While established requirements for stability and control may be useful as design guides, it has been emphasized in reference 6 that it is difficult to include all factors which may be important in the over-all lateral dynamic behavior of an airplane. For example, the airplane's intended mission or peculiarities of a given design may have an important bearing on whether the associated flying qualities will be satisfactory to pilots.

One way of investigating the flying qualities of new designs is to use variable-stability airplanes as flight simulators of the predicted lateral dynamic behavior. In this manner, unusual behavior inherent in a particular design can be investigated in flight long before completion of the prototype; the pilot can become familiar with the lateral dynamic characteristics predicted for the airplane he is later to fly; and problems relating to a given design can be discussed with company engineers who are directly concerned. When this experience is provided in the early stages of design or prototype construction, design modification or installation of artificial-stability equipment can usually be made without causing production delays. To obtain such experience, seven company test pilots have flown the F6F-3 and F-86A variable-stability airplanes in prototype simulation programs at the Ames Aeronautical Laboratory.

It should be noted that these simulation programs were not the usual research-type investigations - techniques varied; no standardized configurations were tested; and results usually differed in type and completeness. In these programs, the variable-stability airplanes served as development tools (in much the same way as wind tunnels) for use by the contractors in connection with their individual prototypes. The purpose of this report is to describe the diverse problems and unique procedures involved and to summarize and discuss qualitatively the results of these flight-simulation programs. In addition, the novel features of the F-86A variable-stability equipment (developed by Mr. H. C. Patton, Jr., of the Ames Aeronautical Laboratory) are discussed.

NOTATION

- A_y lateral acceleration at center of gravity, g units
- $C_{1/2}$ cycles required for lateral oscillation to damp to half amplitude,
 $\frac{T_{1/2}}{P}$
- C_2 cycles required for lateral oscillation to double amplitude, $\frac{T_2}{P}$

C_l rolling-moment coefficient, $\frac{\text{rolling moment}}{qSb}$

$C_{l\beta}$ $\frac{\partial C_l}{\partial \beta}$, per radian

$C_{l\delta_r}$ $\frac{\partial C_l}{\partial \delta_r}$, per radian

C_{lp} $\frac{\partial C_l}{\partial \frac{pb}{2V}}$, per radian

C_{lr} $\frac{\partial C_l}{\partial \frac{rb}{2V}}$, per radian

C_n yawing-moment coefficient, $\frac{\text{yawing moment}}{qSb}$

$C_{n\beta}$ $\frac{\partial C_n}{\partial \beta}$, per radian

$C_{n\delta_a}$ $\frac{\partial C_n}{\partial \delta_a}$, per radian

C_{np} $\frac{\partial C_n}{\partial \frac{pb}{2V}}$, per radian

C_{nr} $\frac{\partial C_n}{\partial \frac{rb}{2V}}$, per radian

C_Y side-force coefficient, $\frac{\text{side force}}{qS}$

$C_{Y\beta}$ $\frac{\partial C_Y}{\partial \beta}$, per radian

D differential operator, $\frac{d}{dt}$

I_{X_0} moment of inertia about longitudinal principal axis, slug-ft²

I_{Z_0} moment of inertia about vertical principal axis, slug-ft²

I_X moment of inertia about longitudinal stability axis,
 $I_{X_0} \cos^2 \eta + I_{Z_0} \sin^2 \eta$, slug-ft²

I_Z	moment of inertia about vertical stability axis, $I_{Z_0} \cos^2 \eta + I_{X_0} \sin^2 \eta$, slug-ft ²
I_{XZ}	product of inertia with respect to longitudinal and vertical stability axes, $(I_{Z_0} - I_{X_0}) \sin \eta \cos \eta$, slug-ft ²
M	Mach number
P	period of lateral oscillation, sec
S	wing area, sq ft
$T_{1/2}$	time required for lateral oscillation to damp to half amplitude, sec
T_2	time required for lateral oscillation to double amplitude, sec
V	true airspeed, ft/sec
V_i	indicated airspeed, knots
V_{S_L}	stalling speed in landing configuration (power off, gear down, high-lift devices at landing setting)
W	weight, lb
b	wing span, ft
g	acceleration due to gravity, 32.2 ft/sec ²
h_p	pressure altitude, ft
i	$\sqrt{-1}$
m	mass, slugs
p	rolling angular velocity, radians/sec
q	dynamic pressure, lb/sq ft
r	yawing angular velocity, radians/sec
t	time, sec
β	sideslip angle, radians
δ_a	total aileron deflection, positive for right aileron down, radians
δ_{ap}	pilot-applied total aileron deflection, radians

δ_r	rudder deflection, positive for trailing edge left, radians
δ_{rp}	pilot-applied rudder deflection, radians
δ_{rs}	servo-applied rudder deflection, radians
η	inclination of the longitudinal principal axis with respect to the flight path, positive when the principal axis is above the flight path at the nose
σ	ratio of air density at test altitude to that at sea level
ϕ	bank angle, radians
$\frac{ \phi }{ \beta }$	ratio of bank-angle amplitude to sideslip amplitude for the oscillatory mode
$\frac{ \phi }{ v_e }$	$\frac{ \phi }{ \beta } \frac{57.3}{v \sqrt{\sigma}}$, $\frac{\text{deg}}{\text{ft/sec}}$
ψ	angle of yaw, radians

EQUIPMENT AND INSTRUMENTATION

Because descriptive material on the variable-stability F6F-3 airplane and servo equipment already has been published, only brief discussions of special additions to the equipment are included in this report. However, since published information on the variable-stability F-86A rudder-servo system is extremely limited, a relatively complete description of that apparatus is presented.

Variable-Stability F6F-3 Airplane

A photograph of the F6F-3 variable-stability airplane used in the simulation programs reported herein is shown in figure 1.

Servo equipment.- The apparatus for varying the dihedral effect of this airplane through servo actuation of the ailerons is described in detail in reference 7. Brief descriptions of similar methods used to vary the stability derivatives C_{n_β} , C_{n_r} , C_{n_p} , and C_{l_p} and to provide simulated rough-air disturbances may be found in references 2 and 8.

In addition to the variable parameters mentioned above, two special features were included for use in studying individual stability and control problems. One provided artificial variation of rolling moment due

to pilot-applied rudder angle $C_{l_{\delta_r}}$; the other allowed servo-applied roll damping C_{l_p} to be varied automatically as a function of lateral stick position. The ways in which these devices were used in the particular simulation programs are discussed later.

Recording instrumentation.- Where data records of specific flight maneuvers were desired, the following quantities were measured: yawing velocity, rolling velocity, sideslip angle, rudder-servo position, aileron-servo position, pilot-applied rudder deflection, and pilot-applied aileron deflection. These quantities were recorded by standard NACA photographic recording instruments synchronized by a 0.1-second instrument timer.

Flight conditions.- All simulation flights in the variable-stability F6F-3 were performed in the clean condition at the following airspeed and altitude:

$$V_i = 200 \text{ knots}$$

$$h_p = 7000 \text{ feet}$$

Variable-Stability F-86A Airplane

A photograph of the F-86A variable-stability airplane is shown in figure 2 and a two-view drawing is presented in figure 3.

Servo equipment.- The F-86A variable-stability servomechanism operates in essentially the same manner as the F6F-3 equipment referenced above. In this airplane, however, only the rudder and rudder tab are driven automatically and the primary power used is hydraulic rather than electric. As in the F6F-3, mechanical differentials are used in the rudder and rudder-tab control systems. The yawing-moment derivatives affected are $C_{n_{\beta}}$, C_{n_r} , C_{n_p} , and $C_{n_{\delta_a}}$. Brief information on the F-86A rudder servo may be found in reference 9.

The rudder servo system installed in the F-86A is of the electro-hydraulic type and incorporates a high-performance single-stage hydraulic valve as the controller. This type of system was selected mainly because of the large servo power requirements at the high airspeeds attainable with this airplane. A simplified block diagram of the electrical-signal portion of the installation is presented in figure 4.

The error-measuring portion of the rudder servomechanism includes a phase-sensitive power amplifier, which senses the difference between the input and follow-up signals. A typical input circuit consists of a

precision-type a-c pickoff, powered by a 400-cycle carrier voltage and mechanically connected to a sensing device, such as a sideslip vane, rate gyro, or pilot's control stick. The output signal from this pickoff is amplified and fed through the pilot's servo-control console, where manual adjustment of servo gearing is made (for example, rudder angle per unit sideslip $\partial\delta_{r_g}/\partial\beta$). The individual signals are then summed, demodulated, and fed into the aforementioned phase-sensitive power amplifier. The resultant amplified error signal is then used to vary the field strength of the servo-valve torque motor, which positions the single-stage valve, driving the hydraulic servo actuator in the desired direction. A follow-up signal proportional to the servo-actuator movement reduces the error voltage to zero when the servo reaches the desired position.

The important components of the hydraulic servo-drive system are shown in figure 5. The system operating pressure is supplied by an engine-driven variable-displacement pump and is regulated to 2700 pounds per square inch by a pressure relief valve. Hydraulic pressure to various parts of the system is controlled by three solenoid-operated two-position valves. Valve 1 (fig. 5) controls pressure to the servo valve (that is, on or off), while valves 2 and 3 control pressure to the servo actuator. The valves are shown energized (pressure on) and the system is shown in normal operation responding to a "right rudder" command signal. Dashed lines represent corresponding valve positions for the pressure-off condition.

During normal shutdown of the system, operation of the hydraulic-pressure switch by the pilot immediately grounds all inputs to the power amplifier, except for the follow-up signal. This causes the rudder servo to drive to a neutral position under normal hydraulic pressure. After a time delay of about 0.15 second, the locking-solenoid plunger (fig. 5) engages the servo-actuator unit and valves 1, 2, and 3 rotate simultaneously to the de-energized position. In the event of failure of airplane primary power, valves 1, 2, and 3 operate immediately and the pilot must engage the locking-solenoid plunger by movement of the pedals in order to return the rudder to neutral.

The mechanical differential used in the combined pilot and servo rudder-control system is shown schematically in figure 5 and a cutaway isometric assembly drawing is presented in figure 6. From these two figures, the desired differential action can be seen. Normal rudder control remains essentially intact; the only alteration was to thread each rudder-control cable from the first guide pulley around the floating center pulley, making a 180° wrap angle, and back through the second guide pulley to the rudder control sector. Thus, if the pedals are held fixed, motion of the floating center pulley results in a proportional displacement of the rudder and, similarly, if the center pulley is fixed, pedal motion results in normal actuation of the rudder. Therefore, any



movement of the rudder (δ_r) is the algebraic sum of the angle called for by the pilot (δ_{rp}) and that caused by displacement of the center pulley (δ_{rs}), which is forced to move with the servo actuator.

The aerodynamic hinge moments due to δ_{rs} , which otherwise would be fed back to the pilot, are balanced by driving the rudder tab in response to motions of the servo. As shown in figure 5, this was accomplished by means of a hydraulic tab actuator connected in series with the rudder-servo actuator. The necessary tab-to-rudder gearing was obtained by proper selection of tab-actuator piston area and by increasing the tab area about 150 percent. Normal tab adjustment by the pilot was retained by mounting the hydraulic tab actuator in series with the production lead-screw-type electric actuator.

Photographs of the variable-stability F-86A cockpit interior, showing the important pilot-operated servo controls, are presented in figure 7. The recording-instrument control units and hydraulic-pressure control switch (on the stick), as well as indicators for sideslip and rudder-servo error signal, are shown in figure 7(a). The rudder-servo control panel is located on the right-hand side of the cockpit and is shown in figure 7(b). Indicators for servo position and hydraulic pressure are included, as well as the servo power switches and knobs for setting the variable-stability parameters. Sine-wave and gust disturbances are provided by deflections of the rudder (through the servo) in response to an electrically driven cam. The F-86A gust generator is similar to that used in the F6F-3, except that signals from two cams driven at different speeds are combined to obtain random inputs. (This method greatly increases the time required for the gust pattern to repeat.) The frequency and amplitude controls for this sine-gust generator are shown in figure 7(b). This figure shows also provision for later installation of an aileron-servo system.

Servo-system operation.- When the F-86A rudder-servo system is operated in flight, the electrical circuits are energized by setting the master-power and rudder-servo switches to the on position. Ammeters which indicate the rudder-servo error signal reduce the possibility of abrupt servo motions which might occur as hydraulic pressure is turned on with large inputs to the servo valve. This error signal may be reduced to zero by the pilot, through use of centering potentiometers located on the servo control panel (fig. 7(b)). The servo drive system is energized when the pilot depresses the hydraulic pressure switch on the control stick. Desired changes in the variable-stability parameters can then be made by setting the selector knobs to appropriate positions. Each knob provides, in addition to the normal F-86A value, four increased values and four reduced values of a particular parameter. Estimated ranges of the F-86A variable-stability parameters (based on control effectiveness and ground-measured servo gearings), as well as those for the F6F-3, are given in table I.



Recording instrumentation.- During flights in the variable-stability F-86A, the following quantities were recorded by means of an 18-channel photographic oscillograph: yawing velocity, rolling velocity, sideslip angle, bank angle, normal acceleration, lateral acceleration, total rudder deflection, rudder-servo position, pilot-applied rudder deflection, total rudder-tab deflection, aileron deflection, rudder-servo error voltage, and rudder-servo follow-up voltage. Standard NACA recording instruments were used to measure pedal force and lateral stick force. The three film records thus obtained were synchronized by means of a 0.1-second instrument timer.

Flight conditions.- Standardized speeds and altitudes used in F-86A variable-stability flight tests are listed as follows:

<u>h_p, ft</u>	<u>M</u>
10,000	0.60
10,000	0.80
35,000	0.80

Variable static and dynamic stability characteristics.- The effects of artificial changes in static directional stability $C_{n\beta}$ on pedal force and displacement as functions of sideslip are shown for the F-86A in figure 8. Time histories of lateral oscillations (returns from steady sideslips, pilot's controls restrained) with various $C_{n\beta}$ and C_{nr} knob settings are presented in figure 9. When attempts are made to change the oscillation period through variations in $C_{n\beta}$ setting alone, large changes in damping also occur. This effect is attributed to changes in C_{nr} resulting from the small phase differences between the β signal and servo-applied rudder deflection δ_{rs} . In order to show the effect of $C_{n\beta}$ setting on period in figure 9 without variations in damping, compensating C_{nr} settings were used as indicated. Similar time histories showing effects of changes in C_{nr} setting alone are presented in figure 10.

SIMULATION PROCEDURE

Predicted controls-fixed lateral oscillatory characteristics and information on any unusual stability or control behavior which might be expected were furnished by the manufacturer in tabular or time-history form. Where these characteristics were not already available, the necessary stability derivatives and mass parameters were obtained from the manufacturer for use in calculating the lateral period, damping, and the ratio of bank angle to equivalent side velocity $|\phi|/|v_e|$. The



method used to calculate the period and damping was similar to that presented in reference 10. The ratio $|\phi|/|\beta|$, from which $|\phi|/|v_e|$ was obtained, was calculated as shown in the appendix by use of the stability system of axes (ref. 10). Flight values of $|\phi|/|\beta|$ were derived from measurements of $|p|/|\beta|$ made with respect to the airplane body axes; however, at the test flight conditions, any discrepancies resulting from the use of different axes systems were considered negligible.

To provide the characteristics of interest, appropriate variable-stability knob settings were chosen from documented results of previous flights or from calibration flights made immediately prior to the simulation. In cases where unusual airplane response to control inputs was anticipated on the prototype, variable-stability settings were selected to give the best approximation of time histories of the predicted motion. With either the F6F-3 or F-86A, it was not possible to duplicate the moments of inertia nor to cover the full range of performance of the simulated airplanes.

Because of the diversity of problems of interest to the various contractors and the specialized techniques required to investigate those problems, no standardized flight procedure or test maneuvers were employed. In all cases, one or two company engineers who were well acquainted with development of the prototype accompanied the visiting test pilot to aid in arranging and evaluating the simulation program.

Following preliminary discussion of the program with the contractor representatives and familiarization of the visiting pilot with the variable-stability airplane and associated servo equipment, the planned simulation flights were made. During these flights, the visiting pilot commented on each condition simulated, either in writing or by radio. Where desired, instrument records of specific flight maneuvers also were obtained.

On completion of the simulation flights, discussions were held with the contractor representatives for the purpose of reviewing the pilot's opinions of the particular conditions simulated and offering suggestions for improvement of marginal or unsatisfactory behavior through possible design changes or artificial stability augmentation.

RESULTS

Airplane A

Airplane A was designed as a high-speed flight-research vehicle powered by two turbojet engines. A two-view drawing and table of principal dimensions of this airplane are presented in figure 11.



The predicted lateral oscillatory characteristics ($1/C_{1/2}$ and $|\phi|/|v_e|$) of airplane A, calculated for several Mach numbers at altitudes of 3,000 and 35,000 feet from stability derivatives and mass parameters furnished by the contractor, are compared in figure 12 with those measured in the variable-stability F6F-3. Although airplane A was not designed as an operational type, the configuration may be representative of future fighter designs. For this reason, the pilot-opinion boundaries of reference 2 are included for comparison. In figure 12, it may be seen that the predicted characteristics of airplane A at all flight conditions considered were well simulated.

As simulated in the F6F-3, all lateral oscillatory characteristics of the basic airplane A corresponding to the 3000-foot altitude were considered satisfactory by the contractor pilot. The characteristics predicted for $M = 0.60$ and 0.90 at 35,000 feet were rated tolerable, while those for $M = 1.00$ were considered intolerable due to the very lightly damped oscillations.

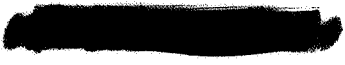
The opinions given by the contractor pilot in the simulation of airplane A tended to be more lenient with regard to high oscillatory roll coupling and low damping than would be indicated by the pilot-opinion boundaries of reference 2. This might be reasonable due to the intended use of airplane A as a research airplane, wherein stringent lateral-oscillation requirements such as those placed on operational aircraft would not be expected to apply. This pilot also had previous flight experience with oscillations having high oscillatory roll coupling and low damping in an earlier research airplane.

Airplane B

A two-view drawing and table of principal dimensions of airplane B are presented in figure 13.

Lateral oscillations.- The lateral oscillatory characteristics of airplane B, calculated for the design cruise ($M = 0.90$, $h_p = 35,000$ feet) and landing-approach conditions by the contractor, are compared in figure 14 with corresponding values of $1/C_{1/2}$ and $|\phi|/|v_e|$ measured in the variable-stability F6F-3 and with the pilot-opinion boundaries of reference 2. Comparison with the boundaries of reference 2 indicated intolerable damping and oscillatory roll-coupling characteristics for the basic airplane B in both the cruise and landing-approach conditions; the contractor was interested in assessing the effects of reducing dihedral effect $C_{l\beta}$ and using a yaw damper to increase C_{nr} in the manner shown in figure 14.

The predicted oscillatory roll-coupling characteristics of airplane B with design $C_{l\beta}$ and three values of C_{nr} were not simulated as closely



as desired; however, the damping in these three cases was represented well by the F6F-3. Figure 14 shows that reasonable simulation of the predicted lateral oscillatory characteristics was provided for the reduced $C_{l\beta}$ conditions.

For the simulated design cruise condition, opinions of the contractor pilot indicated that airplane B would have intolerable lateral oscillatory characteristics. This appeared safe to assume since the opinion was based on an amount of oscillatory roll coupling less than that actually predicted. With one-half design $C_{l\beta}$ and 3 and 6 times design C_{nr} , the resulting characteristics were considered satisfactory. The zero $C_{l\beta}$ condition for all three values of C_{nr} was also rated satisfactory from the lateral-oscillation standpoint but would probably be undesirable for other reasons, which will be discussed later.

No formal opinion was given regarding lateral oscillatory characteristics in the landing-approach configuration; however, an intolerable rating such as that assigned to the basic airplane in the cruise condition would be expected.

Roll due to rudder deflection.- An unusually large value of rolling moment due to rudder deflection $C_{l\delta_r}$ was predicted for airplane B and the contractor was concerned about possible adverse effects on the roll response to abrupt rudder deflections, especially in the landing approach. Analog-computer studies by the contractor indicated initial adverse rolling tendencies in response to rudder step inputs, and a flight investigation of these motions was considered desirable. To investigate this feature, the F6F-3 variable-stability equipment was modified so that $C_{l\delta_r}$ could be varied in flight. This was accomplished by installation of a precision-type a-c pickoff on the pilot's input to the rudder-servo differential; the resulting signal was fed into the aileron servo system through a manual gain control.

The motions indicated by the analog time histories obtained by the contractor were approximated in flight through use of appropriate variable-stability settings in the F6F-3. Figure 15 presents flight time histories of bank angle in response to step-type rudder deflections for the variable-stability F6F-3 set up to simulate airplane B with one-half design $C_{l\beta}$ and with three values of $C_{l\delta_r}$. In each case, sufficient rudder angle was applied to trim the airplane at about 5° sideslip.

As seen from the curve for the normally small $C_{l\delta_r}$ of the F6F-3, figure 15, roll was in the direction expected for positive dihedral effect (left roll for right sideslip) and no initial adverse rolling motion was present. The middle curve indicates the type of rolling motion obtained



in the F6F-3 with a value of $C_{l\delta_r}$ necessary to simulate the response predicted for airplane B. The initial adverse roll shown was noticeable to the pilot but was not considered sufficiently large nor persistent to interfere seriously with control of the airplane. With the planned increase in yaw damping, three times design C_{nr} (not shown), this one-half design $C_{l\beta}$ configuration was considered satisfactory by the contractor pilot and appeared to be a reasonable design goal since a satisfactory rating was also given to the lateral oscillatory characteristics themselves. With the large adverse $C_{l\delta_r}$, the F6F-3 rolled in the adverse direction throughout the maneuver. This continued adverse roll was definitely undesirable in the pilot's opinion.

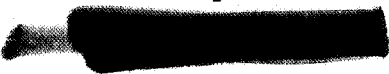
The pilot opinions associated with the motions shown in figure 15 indicated that the limiting case of tolerable adverse $C_{l\delta_r}$ would be one in which no sustained adverse roll occurs for a given value of $C_{l\beta}$. For designs similar to airplane B, this might serve as a rough criterion for determining maximum allowable $C_{l\delta_r}$.

Airplane C

A two-view drawing and table of principal dimensions of airplane C are presented in figure 16.

To provide improved pilot visibility and permit the use of short landing gear by avoiding large fuselage angles of attack during the approach and landing, this carrier-based day fighter featured a two-position variable-incidence wing (-1° incidence for cruise, 7° for landing).

Lateral oscillations.- Calculations made by the contractor for the basic airplane in the landing condition indicated the undesirable lateral oscillatory damping and roll-coupling characteristics shown in figure 17. These characteristics were traced to the predicted high dihedral effect and the lack of favorable positive inclination of the longitudinal principal axis of inertia with respect to the flight-path axis with the wing at 7° incidence. The contractor considered improving these characteristics by means of a yaw damper; calculations indicated that, although a substantial increase in damping could be provided in this manner, the objectionable high value of oscillatory roll coupling would still remain and even increase slightly (fig. 17). Further calculations showed that simultaneous improvements in the damping and roll-coupling characteristics of airplane C in the landing condition could be achieved by means of a roll damper which, through servo actuation of the ailerons in response to a roll-rate gyro, provides large stabilizing increments in the damping-in-roll derivative C_{lp} . The contractor planned to use this type of damper



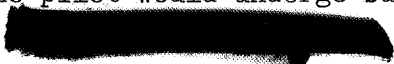
in the landing approach and therefore was interested in comparing its effects with those of a yaw damper on pilot opinions of the associated lateral oscillatory behavior.

It is seen from figure 17 that reasonably good simulation of the predicted characteristics of the basic airplane C (no auxiliary damping) in the landing approach was provided by the F6F-3 for both approach speeds of 1.2 and 1.5 V_{S_L} . Figure 17 also shows that, even though the roll-damper condition at 1.2 V_{S_L} was not simulated as closely as desired, the relative effects of the yaw damper and roll damper were well represented by the F6F-3.

In the opinion of the contractor pilot, the damper-off condition would be intolerable at both approach speeds due to the high oscillatory roll coupling and poor damping. The characteristics associated with the yaw-damper condition at 1.2 V_{S_L} , although deep in the intolerable region of reference 2, were considered marginally satisfactory. The characteristics represented by the simulated roll-damper point were felt to be highly satisfactory due to the large reduction in roll coupling which accompanied increased damping. An additional condition (not shown) represented combined use of the yaw and roll dampers and was considered even more desirable than with the roll damper alone.

Nonlinear roll damper.- While planning the use of a roll damper of the type mentioned, the contractor was aware that roll maneuverability would be impaired due to the high effective C_{l_p} with the roll damper operating. To avoid this, it appeared desirable to vary the roll-damper gain as a nonlinear function of lateral stick position, as suggested in reference 11. In this way, maximum roll damping would be provided in steady flight or in mild maneuvers, and would be reduced to the normal-airplane value when the pilot applied large stick deflections in order to roll rapidly. To obtain pilot opinions of such a nonlinear roll damper, the F6F-3 variable-stability equipment was modified by feeding the rolling-velocity signal to the aileron servo through a tapped potentiometer actuated by the stick. Several symmetric variations of servo-applied C_{l_p} thus were obtained, as shown in figure 18. Results of early flights using this device showed, as expected, that the desired high roll damping and roll maneuverability could be achieved. At the time of the simulation flights for airplane C, the C_{l_p} variation indicated by the solid line (variation 1-3, fig. 18) was considered optimum for rapid roll maneuvers in smooth air by the contractor pilot and two NACA pilots. Subsequent flights by one NACA pilot have indicated that a variation providing full roll damping for moderate stick travel (2-2) might be more suitable for other conditions, such as flying in rough air.

Yaw due to aileron deflection.- Subsequent to the simulation flights made in the F6F-3, analog-computer studies of airplane C by the manufacturer indicated that the pilot would undergo sudden changes in lateral



acceleration of the order of 0.2g immediately following abrupt aileron deflections at high speeds with the rudder fixed. This lateral acceleration resulted largely from yawing acceleration combined with a cockpit location 23 feet ahead of the airplane center of gravity. The initial yawing acceleration was traced to a large favorable variation of yawing moment with aileron deflection $C_{n\delta_a}$ (positive yaw in response to aileron deflection initiating positive roll), a characteristic of certain inboard aileron installations. The contractor felt that this abrupt lateral acceleration would be particularly disturbing to a pilot and hence planned to actuate the rudder in response to aileron deflection (i.e., left rudder for right aileron) over a range of low angles of attack. Analog studies indicated that the lateral-acceleration response would be considerably reduced by this method, and, accordingly, flights were made in the variable-stability F-86A to simulate the predicted behavior of airplane C, both with and without the aileron-rudder interconnection.

Provision for varying $C_{n\delta_a}$ on the variable-stability F-86A in flight had already been made by feeding a signal proportional to lateral stick deflection into the rudder-servo summing amplifier through a manual gain control. Settings for $C_{n\delta_a}$ were chosen on the F-86A which provided close simulation of the lateral-acceleration responses of airplane C (fig. 19). The lateral oscillatory characteristics of airplane C were approximated reasonably well by a moderate reduction in directional stability $C_{n\beta}$.

Opinions of the contractor pilot indicated that the lateral handling qualities of the F-86A set up to simulate the basic condition (without the aileron-rudder interconnection, fig. 19(a)) were not objectionable; in fact, this condition was actually preferred over that simulating the improved condition (with the aileron-rudder interconnection, fig. 19(b)), due to better roll maneuverability which resulted from the favorable sideslip and positive dihedral effect. This opinion was also attributed partly to his previous experience in another fighter-type airplane which exhibited large lateral-acceleration responses (sometimes estimated at 1g) in abrupt aileron rolls. However, during simulated air-to-air gunnery runs (similar to those employed in ref. 8) in the variable-stability F-86A, the contractor pilot encountered more difficulty tracking in the basic configuration than in the improved case. This agreed with gun-camera records and opinions of NACA pilots obtained in subsequent F-86A flights in which the same variable-stability settings were used.

Airplane D

A two-view drawing and table of principal dimensions of airplane D are presented in figure 20.



The predicted lateral oscillatory characteristics of airplane D (measured from analog time histories obtained by the contractor and calculated from stability derivatives and mass parameters furnished by the contractor) are compared in figure 21 with those measured in the variable-stability F6F-3. Several speeds and altitudes, corresponding to power-approach and combat-cruise conditions, are represented. A similar comparison is made between predicted airplane D combat-cruise characteristics simulated in the variable-stability F-86A and the measured F-86A characteristics in figure 22. In both figures 21 and 22, the pilot-opinion boundaries of reference 2 are included for comparison.

In general, simulation of the predicted characteristics of airplane D was satisfactory with both F6F-3 and F-86A variable-stability airplanes. Because of the large number of conditions involved, no attempt was made to simulate each point specifically. Instead, the no-damper conditions of major interest were approximated by a series of conditions (points 1, 4, 6, 9, and 12, fig. 21) having low damping and covering a large range of $|\phi|/|v_e|$. These were then used as basic points to demonstrate the effects of various dampers.

As simulated in the F6F-3 (fig. 21), the combat-cruise, damper-off conditions of airplane D were considered marginal (point 1) to objectionable (point 4) by the contractor pilot on the basis of moderate oscillatory roll coupling combined with low damping. With a yaw damper (approximated by points 2 and 5) these combat-cruise conditions were considered to have satisfactory damping; however, the contractor pilot felt that improvement could be made, especially in rough air, by reducing oscillatory roll coupling through use of lower dihedral effect.

The power-approach, damper-off conditions (points 6, 9, and 12) drew very unfavorable opinions from the contractor pilot because of the high $|\phi|/|v_e|$ and generally poor damping. The addition of a yaw damper in these power-approach conditions (points 7, 10, and 13) increased the damping to an acceptable level. Oscillatory roll coupling $|\phi|/|v_e|$, however, was still considered marginal to objectionable in rough air.

In addition to the yaw-damper conditions, effects of a roll damper (such as proposed for airplane C) were investigated by the contractor pilot in both simulated combat-cruise and power-approach conditions (points 3, 8, and 11, fig. 21). Only a slight effect of the roll damper was noticed in the combat-cruise condition indicated by points 1 and 3, probably because the oscillatory roll coupling without the roll damper was small. In the power-approach condition, the roll-damper effect was considered quite favorable at a speed of $1.4 V_{S_L}$, while at $1.1 V_{S_L}$ only a small improvement over the damper-off condition was noted. In over-all suitability, however, the yaw damper was preferred to the roll damper by the contractor pilot.

All conditions simulated in the variable-stability F-86A (fig. 22) were considered satisfactory from the standpoint of oscillatory roll



coupling. The yaw-damper-off conditions had undesirably low damping, resulting in steady snaking oscillations in rough air, but they were felt to be completely satisfactory with addition of the yaw damper.

Airplane E

A two-view drawing and table of principal dimensions of airplane E (as simulated in the variable-stability F6F-3) are presented in figure 23.

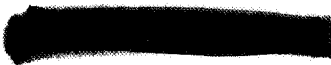
Airplane E was a high-speed bomber configuration for which unusual lateral oscillatory characteristics (long period, unstable oscillations with moderate roll coupling) were predicted in the take-off condition. A second and perhaps more serious problem was a progressive reduction of static directional stability $C_{n\beta}$, which was expected to occur when the design bombing-run Mach number was exceeded by more than 10 percent. Use of a directional stability-augmenting device was planned; however, the contractor was concerned that the resulting long-period unstable lateral oscillation (or even a rapid aperiodic divergence) might be objectionable or dangerous in the event of stability-augmenter failure in this critical flight condition.

In the F6F-3, variable-stability knob settings were chosen to simulate the predicted lateral oscillatory characteristics of interest and the available range of reduced $C_{n\beta}$ was extended to provide the desired simulation of low static directional stability.

Lateral oscillations.- The predicted lateral oscillatory characteristics of airplane E (calculated by the contractor and the NACA) are compared in figure 24 with those measured in the F6F-3. Simulation of the predicted oscillatory characteristics in the take-off condition ($M = 0.35$, $h_p = 0$) and after refueling ($M = 0.60$, $h_p = 30,000$ feet) was reasonably good. The remaining conditions at high speeds and high altitudes (still with positive $C_{n\beta}$) were not simulated as well as desired.

In the opinion of the contractor pilot, the lateral oscillatory characteristics predicted for the take-off condition were intolerable. This opinion was based on the divergent oscillation, which was felt to be especially objectionable in view of anticipated flight near ground level. The remaining conditions, as experienced in the F6F-3, were considered tolerable from the lateral-oscillation standpoint.

Low directional stability.- Some effects of neutral static directional stability are shown in figure 25. Presented are time histories of pilot-applied control deflections and airplane motions with cockpit controls held fixed and with the pilot attempting to hold a steady course in simulated instrument flight. Under controls-fixed conditions, the airplane motion



involved an unstable lateral oscillation of very long period ($P \approx 14$ sec). Figure 25 also shows that reasonably steady flight could be maintained under instrument conditions; however, considerable attention to aileron and rudder control was required. In general, the contractor pilot felt that flight of the variable-stability F6F-3 in the region around neutral directional stability (where $T_2 \approx 12$ sec) was not necessarily dangerous but would be bothersome and fatiguing over extended periods of time.

Subsequent to the simulation program involving the F6F-3, changes in the design of airplane E had been made. The low directional-stability problem was still expected to occur in the high-speed cruise condition and, in addition, strong favorable $C_{n_{\delta_a}}$ (as in the case of airplane C) and low roll damping C_{l_p} were indicated by wind-tunnel tests and preliminary calculations. The contractor was interested mainly in obtaining some indication of minimum acceptable C_{n_β} with stability-augmenting devices inoperative in the high-speed cruise condition, in the presence of predicted $C_{n_{\delta_a}}$ and C_{l_p} . The variable-stability F-86A was chosen as the test vehicle in this case because of its greater speed and altitude capabilities. A two-view drawing and table of principal dimensions of airplane E as simulated in the variable-stability F-86A are presented in figure 26.

At the test flight conditions of $M = 0.80$ and $h_p = 35,000$ feet, F-86A variable-stability knob settings were chosen to give the best approximation of predicted controls-fixed lateral oscillatory behavior of airplane E. Since the variable-stability F-86A was not equipped with an aileron servo drive system, it was not possible to make significant changes in the roll-damping derivative C_{l_p} . However, C_{n_p} was artificially varied to give the pilot an impression of low roll damping. This was accomplished by selecting a C_{n_p} servo gearing which provided, for example, a right yawing moment in response to a right roll initiated by the pilot. This in turn resulted in a left sideslip and an additional right rolling moment due to positive dihedral effect, giving the desired end effect of an increase in roll velocity for a given stick deflection (at least during the middle portion of the roll transient). Through proper selection of $C_{n_{\delta_a}}$ and C_{n_p} gearings, in addition to C_{n_r} and C_{n_β} , it was possible to obtain a reasonable simulation of the over-all lateral and directional response to control inputs predicted for airplane E.

Once the appropriate variable-stability servo gearings had been established, a series of flights were made in which the contractor pilot explored the interesting range of low directional stability C_{n_β} . From these flights, the pilot first concluded that a value of C_{n_β} corresponding to 25 to 30 percent of that of the normal F-86A was about the minimum acceptable. However, as he gained experience in this region of C_{n_β} , he felt that still lower values might be tolerated. In cases where



wide differences in mass and performance characteristics of the simulator and simulated airplanes are involved, such as in the present example, it would not appear wise to apply values of critical stability derivatives (such as minimum $C_{n\beta}$) estimated in the simulation flights as direct numerical criteria in the prototype design.

Airplane F

A two-view drawing and table of principal dimensions of airplane F are presented in figure 27.

Airplane F was designed as a two-place, jet-powered trainer which could accommodate variable-stability servo equipment for the purpose of simulating dynamic behavior of modern fighter aircraft about all three stability axes. The contractor pilot flew the F6F-3 to gain familiarity with the variable-stability concept and for simulation of the predicted lateral oscillatory characteristics of airplane F.

The predicted lateral oscillatory characteristics of airplane F, calculated by the contractor for sea-level climb and landing conditions, are compared in figure 28 with those measured in the variable-stability F6F-3. Although airplane F was not a fighter type itself, the pilot-opinion boundaries of reference 2 are included for simple comparison.

The characteristics represented by the F6F-3 points in figure 28 were evaluated by the contractor pilot both in smooth air and with the rough-air simulator (ref. 8) set at moderate aileron and rudder amplitudes. The pilot considered the simulated lateral-oscillatory characteristics of airplane F in the climb condition (point 1, fig. 28) to be satisfactory, since good damping was present and he was able to hold a steady course in simulated rough air. Points 2 and 3 of figure 28 bracketed the predicted damping characteristics of airplane F in the landing condition; the pilot rated point 2 as he did point 1 - very good damping and easy to hold on course in rough air. Point 3 was acceptable, though becoming difficult to control in rough air, having marginally satisfactory damping. The very low roll coupling of airplane F in the climb condition could not be simulated as closely as desired without the use of objectionable negative dihedral effect on the F6F-3; however, previous pilot-opinion studies indicate that such differences in roll coupling are not critical in the range considered (ref. 2). Close simulation of the oscillation period in the landing condition was sacrificed in order to preserve much of the high directional stability still present in that condition.

In addition to the lateral oscillatory characteristics presented in figure 28, analog time histories furnished by the contractor showed marked spiral divergence of airplane F in the landing condition. Accordingly,



F6F-3 variable-stability settings providing mild to substantial spiral divergence were included in this flight program, but no exact simulation of the computed divergence of airplane F was attempted.

DISCUSSION

The results of these various simulation programs have been discussed individually as they were presented. The present section provides a recapitulation of the more important information and experiences gained during these programs. Pilot opinions of the lateral oscillatory characteristics, an item of importance common to nearly all the airplanes studied, are discussed first; then follow the special problems which were of interest usually in individual cases.

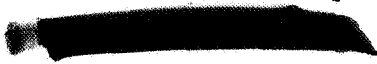
Lateral Oscillatory Characteristics

Written and verbal opinions expressed by the contractor pilots concerning the lateral oscillatory characteristics of airplanes A, B, C, D, and F (as simulated with the variable-stability F6F-3) have been assembled and are shown qualitatively by the shaded areas in figure 29. Included are the pilot-opinion boundaries of reference 2 and those presented in the current military specification (ref. 1).

The comments indicated by the shaded areas were obtained from information volunteered by each pilot during and immediately following the simulation flights. No formal procedure was used for obtaining pilot opinions; the pilots were not requested to answer standardized questions or to perform specific maneuvers. In most cases, the flight procedure was dictated by the particular problem being investigated.

In substance, reference 1 states that airplanes in the clean or the landing configuration (while not engaged in gunnery, bombing, or other critical duties) must have, in controls-fixed and controls-free lateral-directional oscillations, a value of the damping parameter $1/C_{1/2}$ not less than that represented by curve a of figure 29. Reference 1 states further that if an artificial stabilization device is employed, $1/C_{1/2}$ with the device inoperative shall be at least 0.24 in all configurations, and shall be at least that represented by curve b in the power-approach configuration. In view of this consideration of artificial-stability devices, direct comparison between the two sets of boundaries presented in figure 29 is difficult because reference 2 considers only normal operation of fighter-type airplanes.

Most of the airplanes considered in figure 29 had predicted damping characteristics below boundary b of reference 1 only in the landing-approach configuration. All the contractor pilots indicated that lateral



oscillatory behavior characterized by shaded area 3 would require stability augmentation in the landing approach; however, they did not indicate specifically that such behavior would be unsatisfactory for a condition of damper failure. It may be that in a detailed pilot-opinion survey (with appropriate questionnaire, rating scale, and flight procedure) such "emergency" considerations would result in less damping required for satisfactory behavior than is specified by boundary b. Since the pilot-opinion data of figure 29 were among those considered in arriving at the lateral-oscillation specification of reference 1, the good agreement between the pilots' comments and boundaries a and b is not surprising.

It should be noted that the characteristics represented in figure 29 involve only lateral-oscillation periods greater than 1.9 seconds (the minimum normally attainable with the variable-stability F6F-3). As indicated in reference 4, shorter periods associated with high-speed flight at medium and low altitudes may place more stringent requirements on damping and oscillatory roll coupling.

Special Problems

Design information related to particular stability and control problems (other than lateral oscillatory behavior) investigated during these simulation programs is summarized in the following paragraphs.

Roll due to rudder deflection.- Airplanes having unusually high values of $C_{l\delta_r}$ may exhibit adverse rolling tendencies in response to rudder deflections (such as those predicted for airplane B), particularly if dihedral effect is low. Pilot opinions associated with such motions simulated in the variable-stability F6F-3 indicated that the limiting case of tolerable adverse $C_{l\delta_r}$ would be one in which no sustained adverse roll occurs for a given value of $C_{l\beta}$. This might serve as a rough criterion for maximum allowable $C_{l\delta_r}$ for designs similar to airplane B.

Yaw due to aileron deflection.- In the variable-stability F-86A, yawing motions similar to those excited by deflection of inboard ailerons (airplane C) were found to make air-to-air tracking difficult. Reduction of these motions, simulating the effect of an aileron-rudder interconnection, brought about improvement in tracking performance.

Nonlinear roll damper.- For certain airplanes (e.g., airplane C), use of a roll (C_{l_p}) damper to provide improved damping and reduced oscillatory roll coupling in the landing approach appears promising. Pilot opinions obtained in flights of the variable-stability F6F-3 indicated that reduction of damper-applied C_{l_p} with lateral stick deflection is desirable in



order to maintain good roll performance. The manner in which C_{l_p} should be varied with stick deflection appears to be similar to that shown by curve 1-3 or 2-2 of figure 18.

Low directional stability.- Tests made in the variable-stability F6F-3 and F-86A indicated that substantial reductions in directional stability C_{n_β} could be tolerated, though it was felt that flight under such conditions for extended periods of time would be fatiguing to a pilot. During flights in the F-86A, values of C_{n_β} as low as 25 percent of the normal value were tolerated. Caution should be used, however, in applying figures such as this as direct design criteria when wide differences in mass and performance characteristics occur between the simulator and prototype airplanes.

CONCLUDING REMARKS

Through use of the NACA variable-stability F6F-3 and F-86A airplanes, flight experience was obtained with lateral dynamic characteristics representative of those predicted for six prototype airplanes. From these studies, it was found that where unusual stability or control-response characteristics were predicted, or where auxiliary damping devices were to be employed, the test pilots who were to fly these airplanes gained familiarity with the trends in lateral behavior and were able to define ranges of acceptable characteristics. The flight experience obtained was in most cases directly applied to particular flying-qualities problems associated with the individual prototype development programs.

In the investigation of new fighter designs by means of variable-stability airplanes, higher performance airplanes should be used because of the greater speed capabilities and, hence, shorter oscillation periods attainable. This would allow more satisfactory simulation of high-speed lateral oscillatory characteristics than could be provided by the variable-stability F6F-3.

Ames Aeronautical Laboratory
National Advisory Committee for Aeronautics
Moffett Field, Calif., Mar. 8, 1956



APPENDIX

METHOD USED TO CALCULATE $|\phi|/|\beta|$

The lateral-oscillation bank-to-sideslip ratio $|\phi|/|\beta|$ was calculated, neglecting effects of airframe flexibility, from the following three linearized equations of motion referred to the stability system of axes presented in reference 10 (for level flight):

Rolling moment

$$(A_1 D^2 + A_2 D)\phi + (A_4 D^2 + A_5 D)\psi + A_9 \beta = A_{10} \quad (1)$$

Yawing moment

$$(B_1 D^2 + B_2 D)\phi + (B_4 D^2 + B_5 D)\psi + B_9 \beta = B_{10} \quad (2)$$

Side force

$$C_3 \phi + C_5 D \psi + (C_8 D + C_9) \beta = C_{10} \quad (3)$$

where

$$A_1 = I_X$$

$$A_2 = -qSb(b/2V)C_{l_p}$$

$$A_4 = I_{XZ}$$

$$A_5 = -qSb(b/2V)C_{l_r}$$

$$A_9 = -qSbC_{l_\beta}$$

$$B_1 = I_{XZ}$$

$$B_2 = -qSb(b/2V)C_{n_p}$$

$$B_4 = I_Z$$

$$B_5 = -qSb(b/2V)C_{n_r}$$

$$B_9 = -qSbC_{n_\beta}$$

$$C_3 = -W$$

$$C_5 = C_8 = mV$$

$$C_9 = -qSC_{Y_\beta}$$

A_{10} = rolling-moment disturbance = 0

B_{10} = yawing-moment disturbance = 0

C_{10} = side-force disturbance

Solutions for ϕ and β , respectively, in response to a unit side-force disturbance, are expressed as

$$\phi = \frac{\begin{vmatrix} 0 & A_4 D^2 + A_5 D & A_9 \\ 0 & B_4 D^2 + B_5 D & B_9 \\ 1 & C_5 D & C_8 D + C_9 \end{vmatrix}}{F(D)} \quad (4)$$

$$\beta = \frac{\begin{vmatrix} A_1 D^2 + A_2 D & A_4 D^2 + A_5 D & 0 \\ B_1 D^2 + B_2 D & B_4 D^2 + B_5 D & 0 \\ C_3 & C_5 D & 1 \end{vmatrix}}{F(D)} \quad (5)$$

where

$$F(D) = \begin{vmatrix} A_1 D^2 + A_2 D & A_4 D^2 + A_5 D & A_9 \\ B_1 D^2 + B_2 D & B_4 D^2 + B_5 D & B_9 \\ C_3 & C_5 D & C_8 D + C_9 \end{vmatrix} \quad (6)$$

Expanding the determinants, dividing expression (4) by expression (5), and simplifying results in

$$\frac{\phi}{\beta} = \frac{(A_4 B_9 - A_9 B_4)D + (A_5 B_9 - A_9 B_5)}{(A_1 B_4 - A_4 B_1)D^3 + (A_1 B_5 - A_5 B_1 + A_2 B_4 - A_4 B_2)D^2 + (A_2 B_5 - A_5 B_2)D} \quad (7)$$

For the free oscillation, let $D = a + ib$, where a and b are the real and imaginary parts, respectively, of the complex roots of the characteristic equation (from $F(D) = 0$). Then

$$D^2 = a^2 - b^2 + 2abi$$

and

$$D^3 = a^3 - 3ab^2 + (3a^2b - b^3)i$$

Expression (7) then reduces to:

$$\frac{\varphi}{\beta} = \frac{Q_1 + iR_1}{Q_2 + iR_2} \quad (8)$$

where

$$Q_1 = a(A_4B_9 - A_9B_4) + (A_5B_9 - A_9B_5)$$

$$R_1 = b(A_4B_9 - A_9B_4)$$

$$Q_2 = (a^3 - 3ab^2)(A_1B_4 - A_4B_1) + \\ (a^2 - b^2)(A_1B_5 - A_5B_1 + A_2B_4 - A_4B_2) + \\ a(A_2B_5 - A_5B_2)$$

$$R_2 = (3a^2b - b^3)(A_1B_4 - A_4B_1) + \\ 2ab(A_1B_5 - A_5B_1 + A_2B_4 - A_4B_2) + \\ b(A_2B_5 - A_5B_2)$$

The ratio of the amplitudes of φ and β at a given instant of time during the oscillation is then expressed as

$$\frac{|\varphi|}{|\beta|} = \sqrt{\frac{Q_1^2 + R_1^2}{Q_2^2 + R_2^2}} \quad (9)$$

The parameter $|\varphi|/|v_e|$ was then calculated using the relation

$$\frac{|\varphi|}{|v_e|} = \frac{|\varphi|}{|\beta|} \frac{57.3}{v\sqrt{\sigma}}$$

REFERENCES

1. Anon.: Military Specification - Flying Qualities of Piloted Airplanes. MIL-F-8785(ASG), Sept. 1, 1954. (Amendment 1, Oct. 19, 1954).
 2. Liddell, Charles J., Jr., Creer, Brent Y., and Van Dyke, Rudolph D., Jr.: A Flight Study of Requirements for Satisfactory Lateral Oscillatory Characteristics of Fighter Aircraft. NACA RM A51E16, 1951.
 3. Bull, Gifford: A Flight Investigation of Acceptable Roll to Yaw Ratio of the Dutch Roll, and Acceptable Spiral Divergence. Rep. No. TB-574-F-6, Cornell Aero. Lab., Inc., Buffalo, Feb. 12, 1952.
 4. Moore, Norton B.: Artificial Stability Flight Tests of the XF-88A Airplane. TR 52-298, Wright Air Dev. Center, July, 1954.
 5. Graham, Dunstan, and James, Clarence W.: A Flight Investigation of Minimum Acceptable Lateral Dynamic Stability. Rep. No. TB-574-F-3, Cornell Aero. Lab., Inc., Buffalo, Apr. 30, 1950.
 6. Kauffman, William M., and Drinkwater, Fred J., III: Variable-Stability Airplanes in Lateral-Stability Research. Aeronautical Engineering Review, vol. 14, no. 8, Aug. 1955, pp. 29-35.
 7. Kauffman, William M., Liddell, Charles J., Jr., Smith, Allan, and Van Dyke, Rudolph D., Jr.: An Apparatus for Varying Effective Dihedral in Flight with Application to a Study of Tolerable Dihedral on a Conventional Fighter Airplane. NACA Rep. 948, 1949.
 8. McNeill, Walter E., Drinkwater, Fred J., III, and Van Dyke, Rudolph D., Jr.: A Flight Study of the Effects on Tracking Performance of Changes in the Lateral-Oscillatory Characteristics of a Fighter Airplane. NACA RM A53H10, 1953.
 9. Smith, G. Allan, and Belsley, Steven E.: Artificial Lateral Aircraft Stability by Servo Control and Some Artificial Feel Experiments. BuAer. Rep. AE-61-5 pt. 1, Report of the Second Piloted Aircraft Flight Control System Symposium, June 2-5, 1952, pp. 47-63.
 10. Heinle, Donovan R., and McNeill, Walter E.: Correlation of Predicted and Experimental Lateral Oscillation Characteristics for Several Airplanes. NACA RM A52J06, 1952.
 11. Schade, Robert O., and Hassell, James L., Jr.: The Effects on Dynamic Lateral Stability and Control of Large Artificial Variations in the Rotary Stability Derivatives. NACA Rep. 1151, 1953 (Supersedes NACA TN 2781).
- 

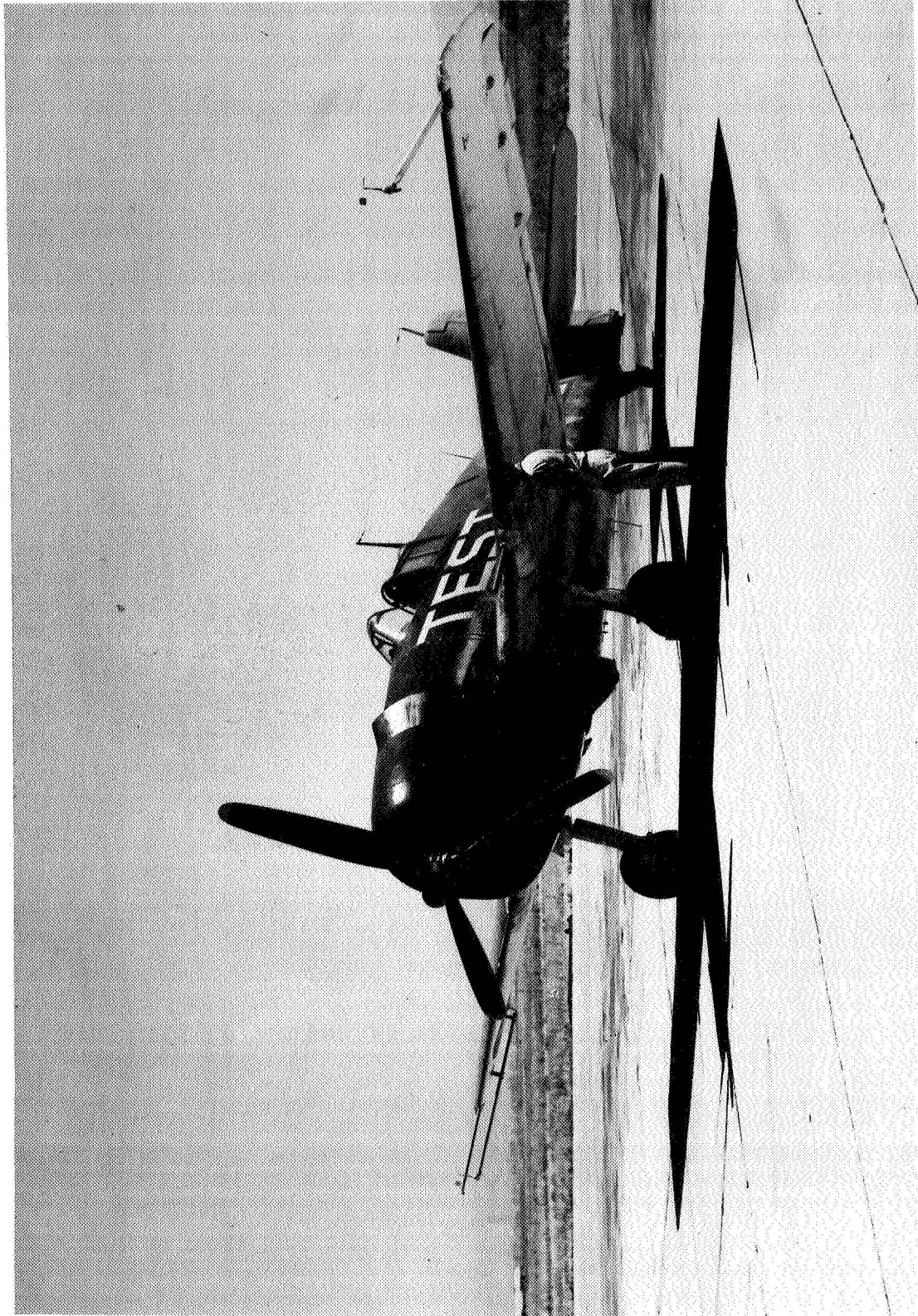
TABLE I.- ESTIMATED RANGES OF VARIABLE STABILITY AND CONTROL PARAMETERS
AVAILABLE ON F6F-3 AND F86-A AIRPLANES

Parameter	F6F-3			F-86A ¹		
	Maximum	Normal	Minimum	Maximum	Normal	Minimum
$C_{n\beta}$	0.079	0.030	-0.002	0.50	0.127	0
C_{nr}	.143	-.080	-.306	.38	-.197	-1.6
C_{np}	.250	-.011	-.151	.34	-.012	-.10
$C_{l\beta}$.048	-.080	-.350	---	-.074	---
C_{lp}	.125	-.450	-1.02	---	-.385	---
$C_{n\delta_a}$	---	.007	---	-.016	.008	.104
$C_{l\delta_r}$.118	0	0	---	.0155	---

¹M = 0.80 at $h_p = 35,000$ ft

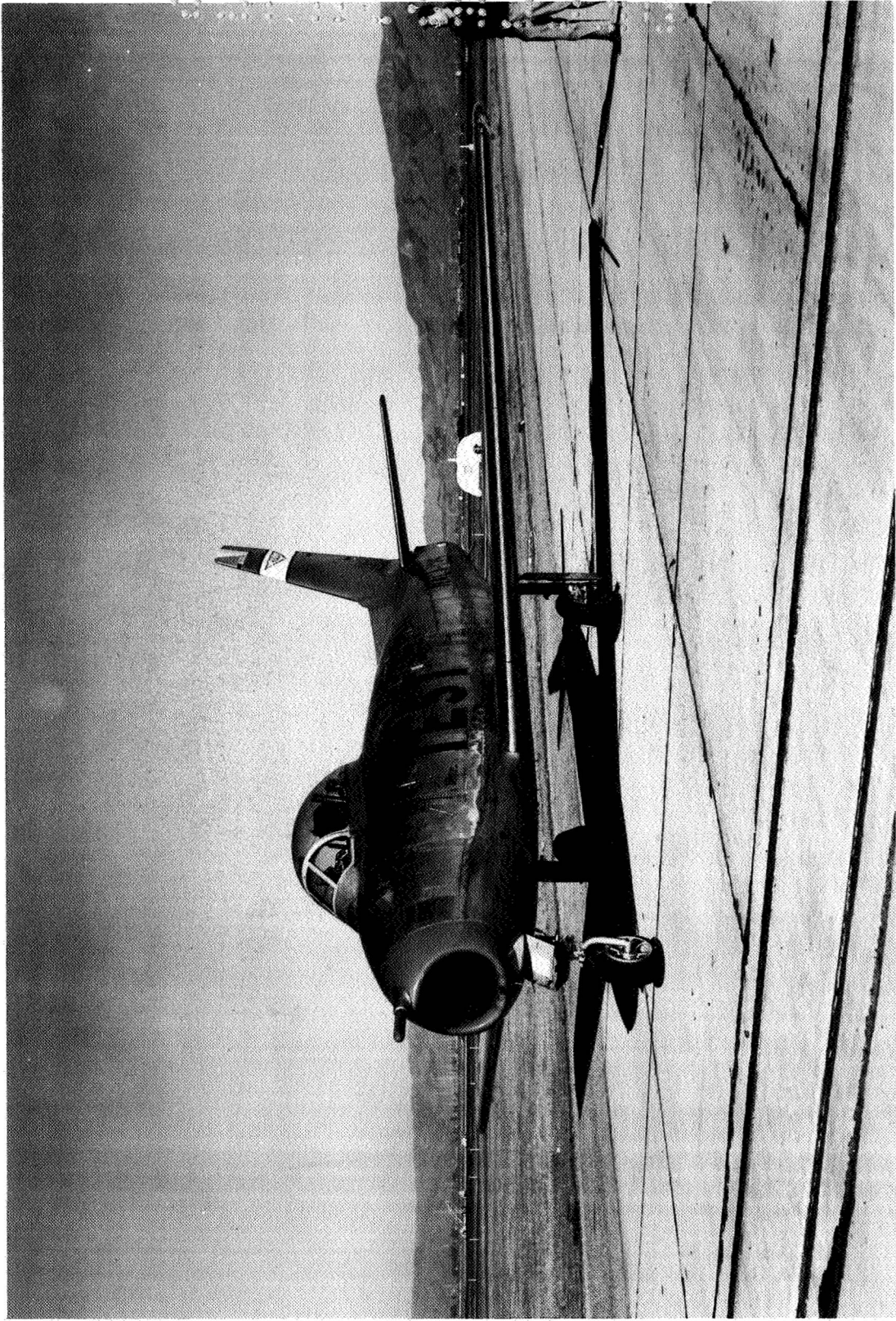
CONFIDENTIAL





A-13080

Figure 1.- Three-quarter front view of variable-stability F6F-3 airplane.



A-20015

Figure 2.- Three-quarter front view of variable-stability F-86A airplane.

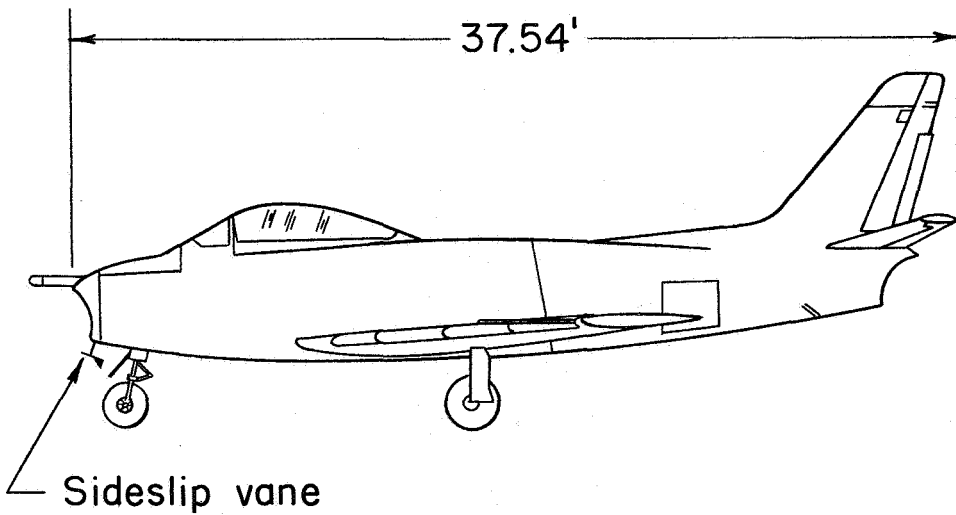
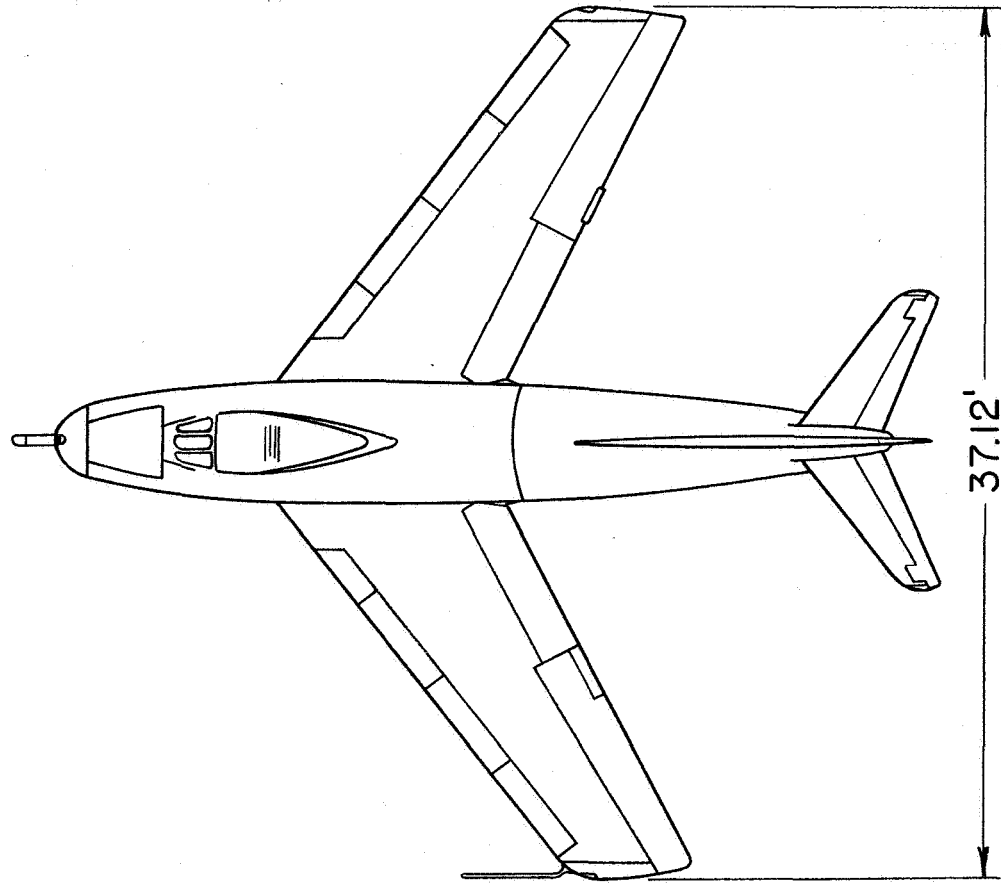


Figure 3.- Two-view drawing of the variable-stability F-86A airplane.



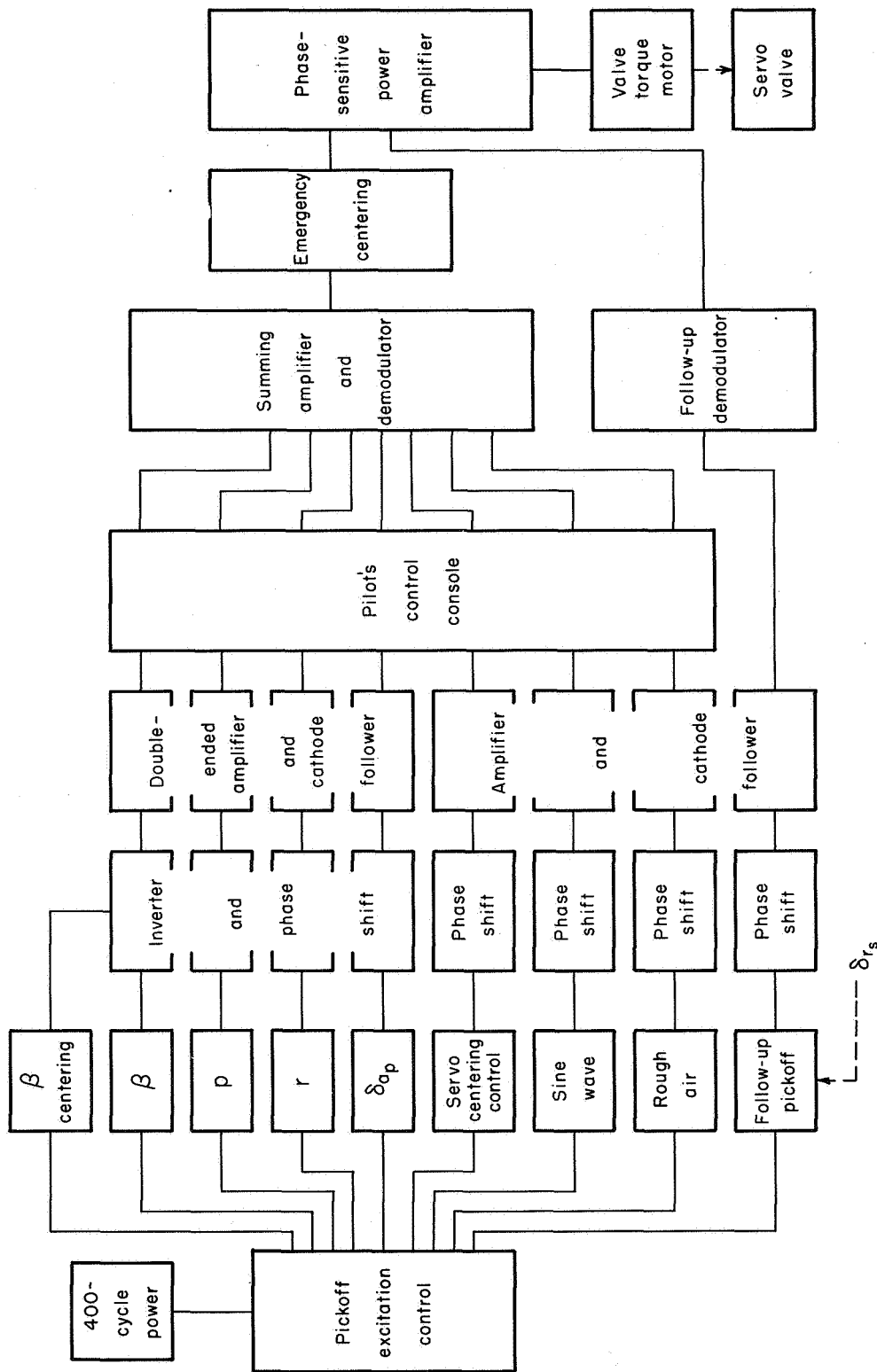


Figure 4.- Block diagram of variable-stability F-86A rudder-servo electrical system

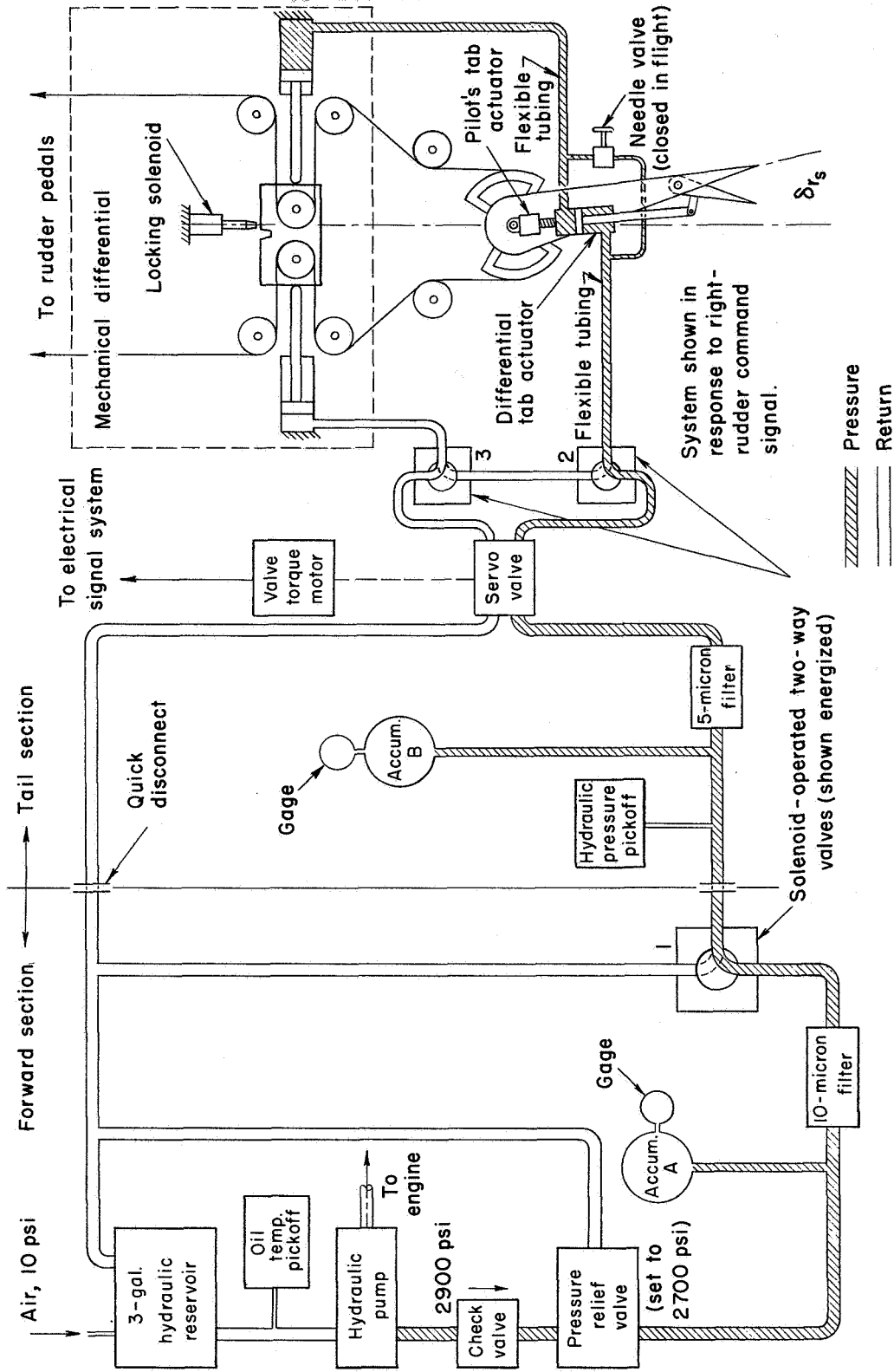


Figure 5.- Schematic diagram of variable-stability F-86A rudder-servo hydraulic system.

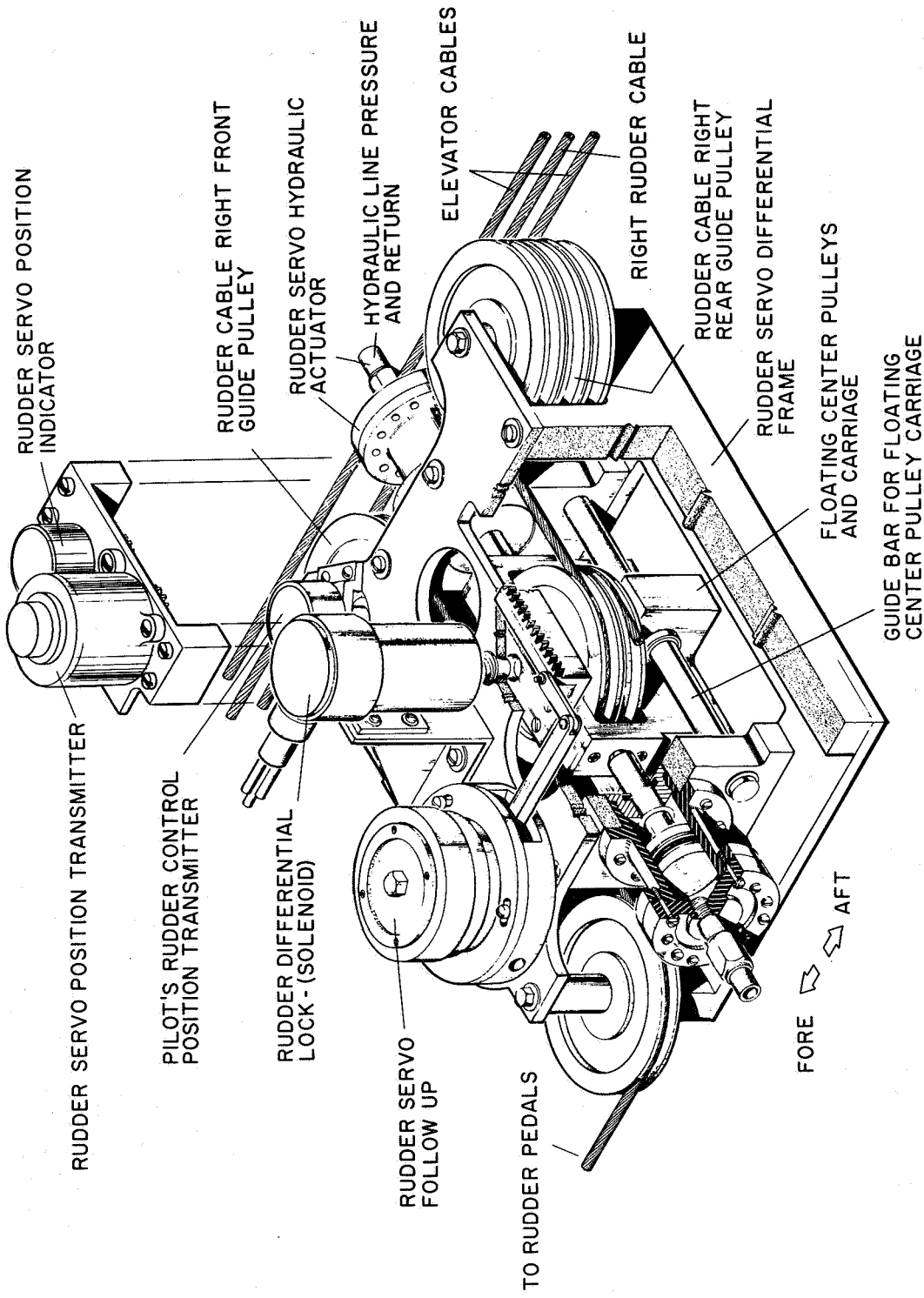
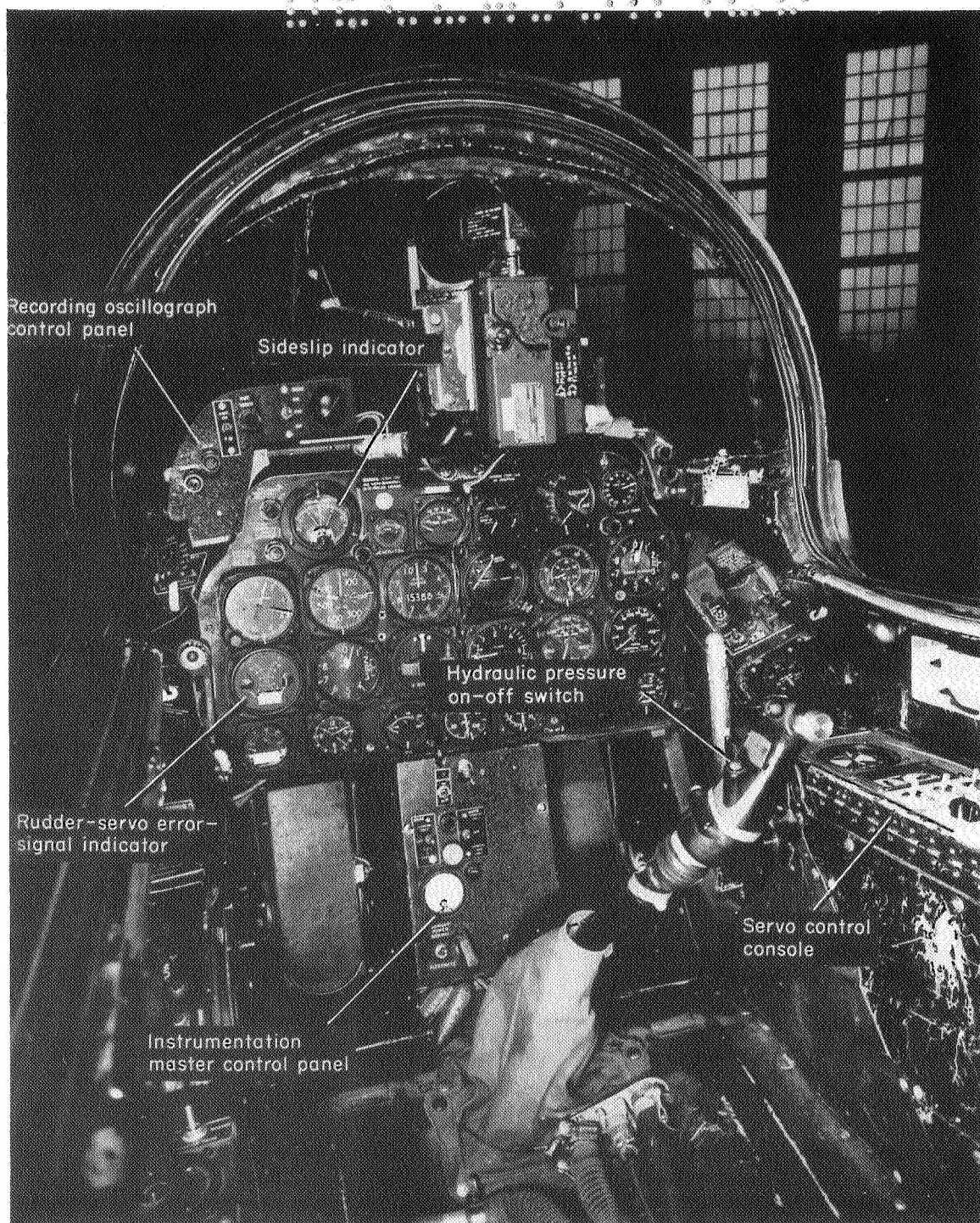


Figure 6.- Variable-stability F-86A rudder-servo differential.

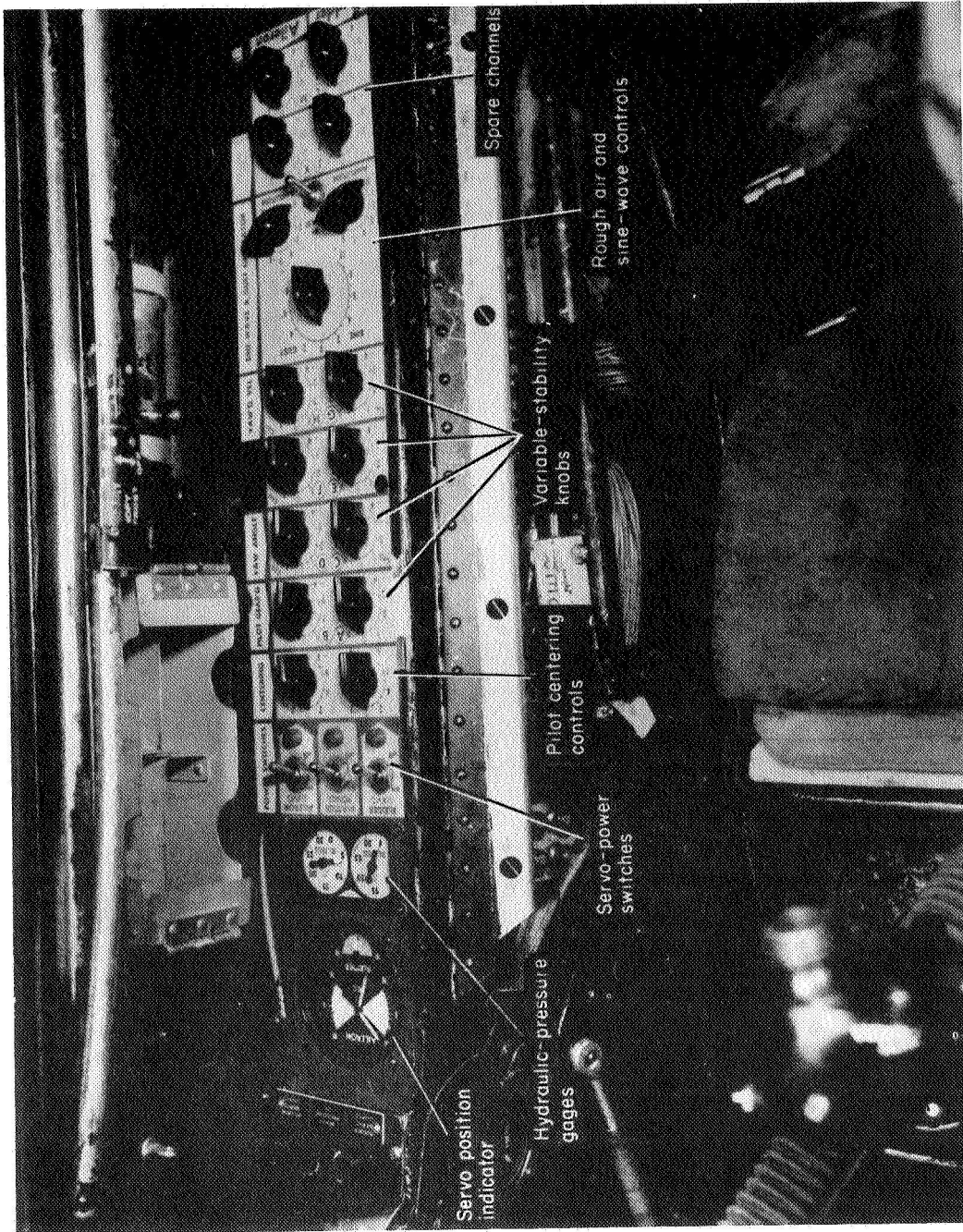


A-20020.1

(a) Facing forward.

Figure 7.- Views of variable-stability F-86A cockpit interior showing instrumentation and servo control components.





A-18803.1

(b) Rudder-servo control console, right-hand side of cockpit.

Figure 7.- Concluded.

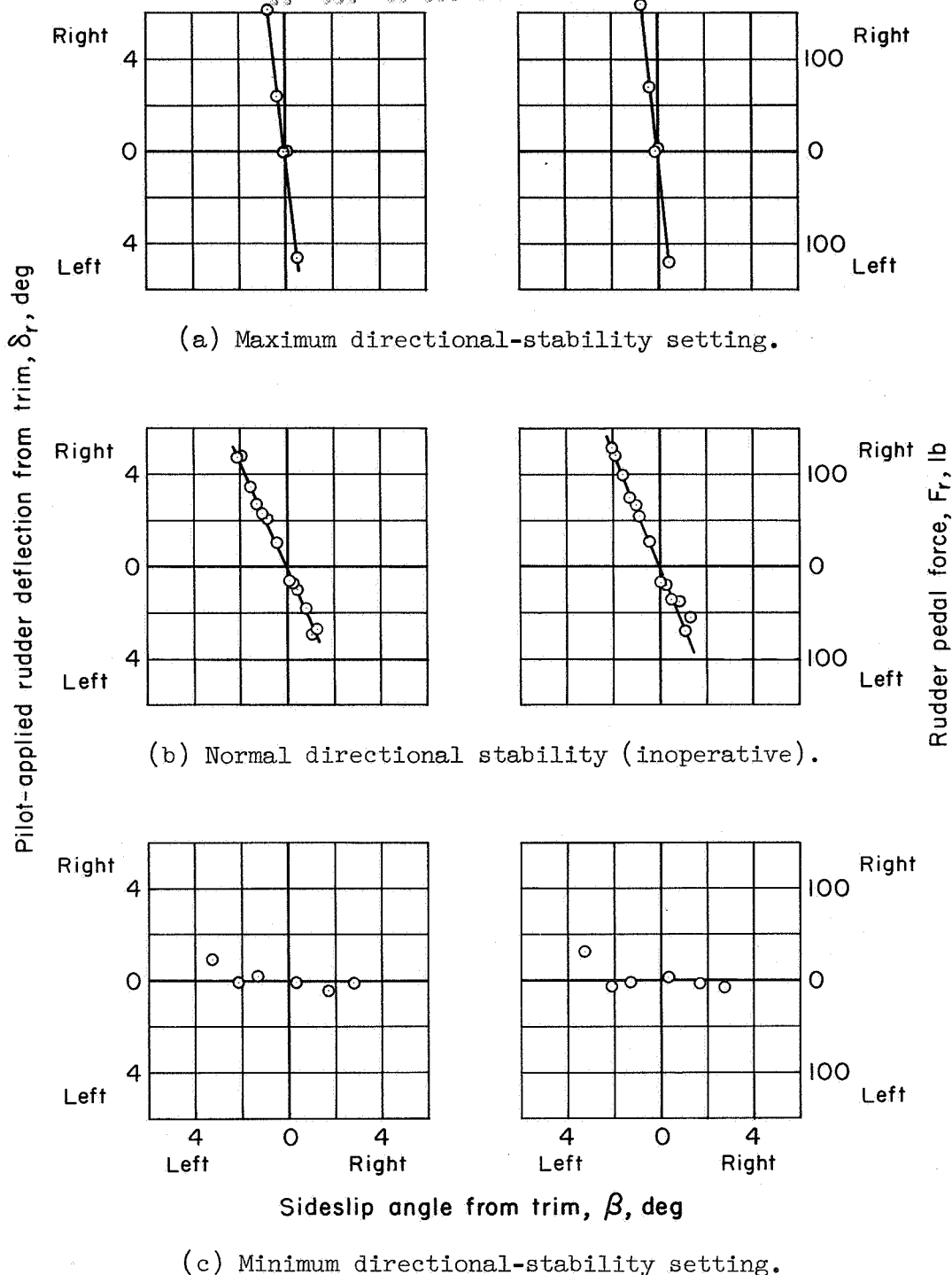
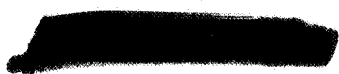
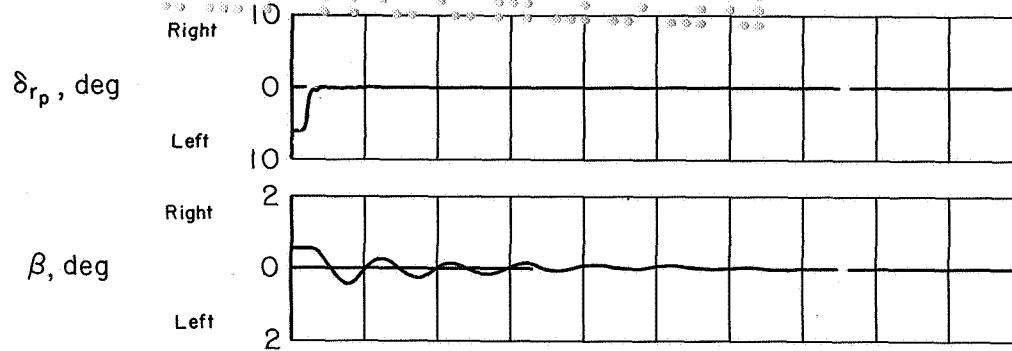
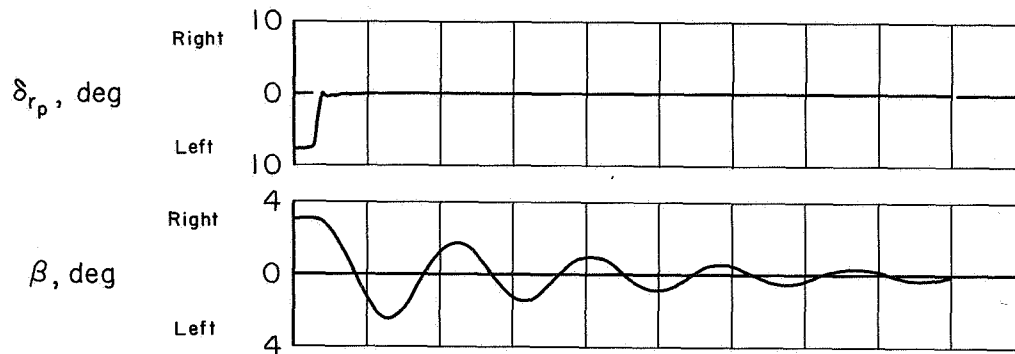


Figure 8.- Directional stability and control characteristics during steady, straight sideslips; variable-stability F-86A, $M = 0.80$, $h_p = 35,000$ feet.

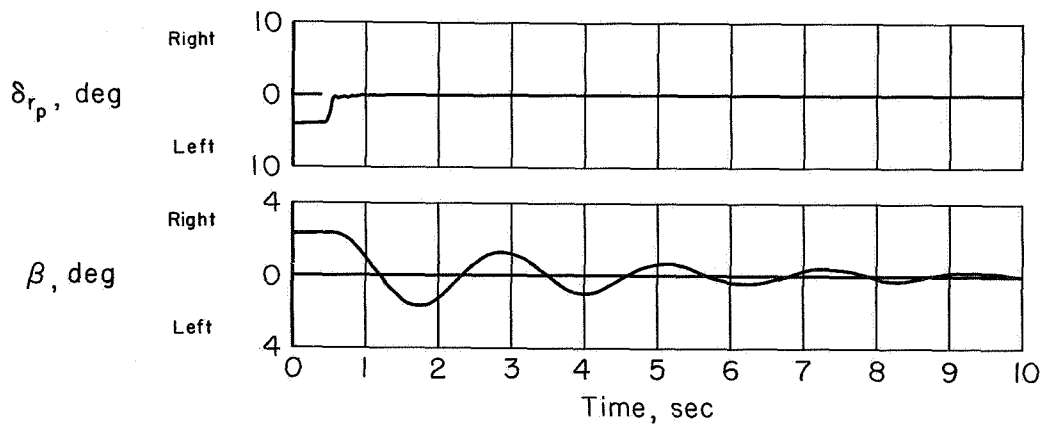




(a) Directional-stability setting: maximum stabilizing.
Directional-damping setting: maximum stabilizing.

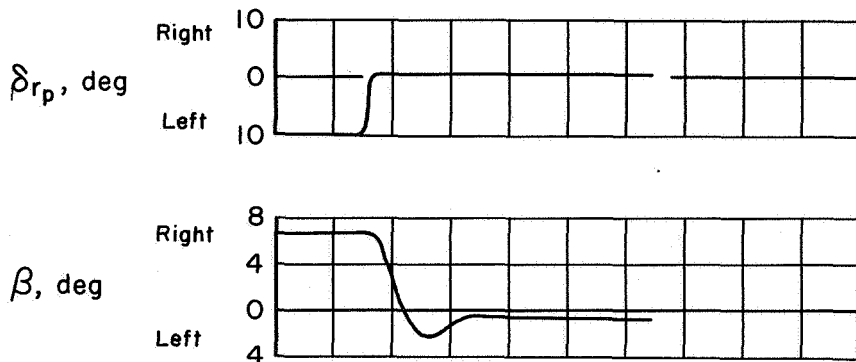


(b) Directional-stability setting: normal (inoperative).
Directional-damping setting: normal (inoperative).

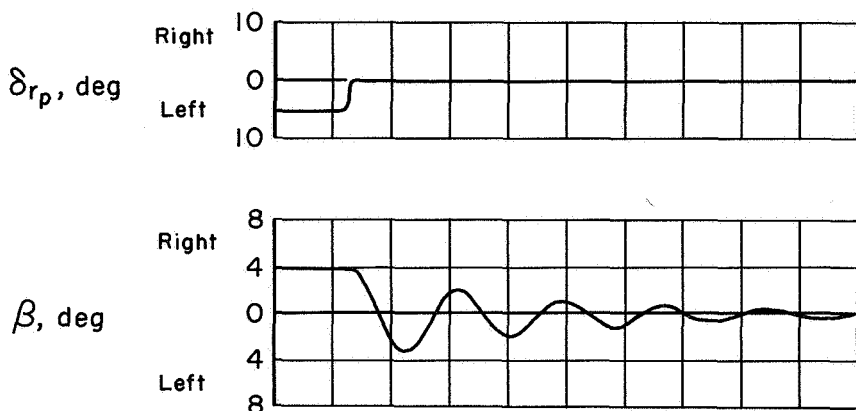


(c) Directional-stability setting: intermediate destabilizing.
Directional-damping setting: intermediate destabilizing.

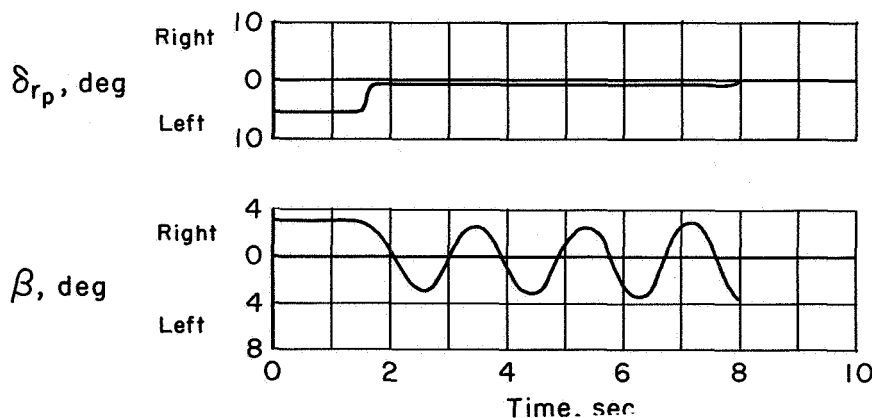
Figure 9.- Time histories of typical controls-fixed lateral oscillations with yaw due to roll rate normal; variable-stability F-86A, $M = 0.80$, $h_p = 35,000$ feet.



(a) Directional damping: intermediate stabilizing.



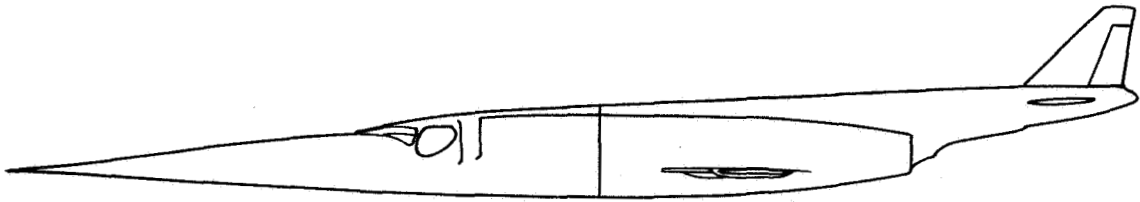
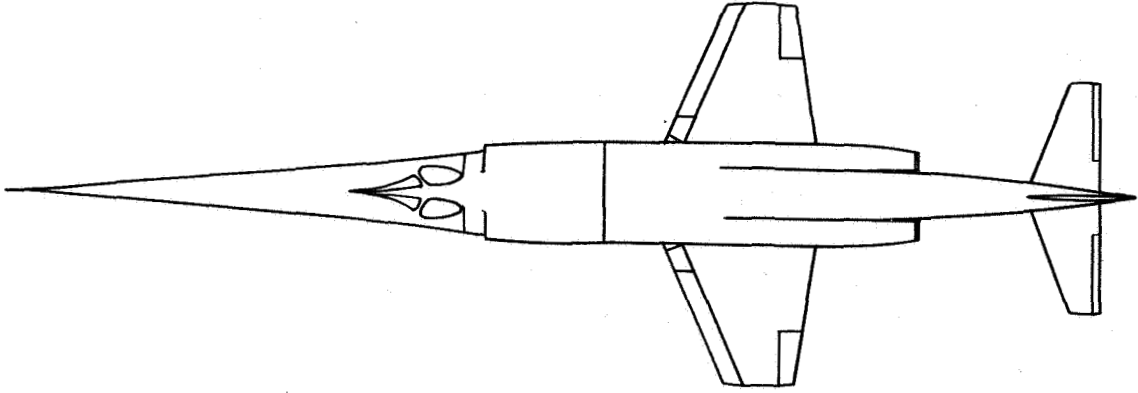
(b) Directional damping: normal (inoperative).



(c) Directional damping: intermediate destabilizing.

Figure 10.- Time histories of typical controls-fixed lateral oscillations with directional stability and yaw due to roll rate normal; variable-stability F-86A, $M = 0.80$, $h_p = 35,000$ feet.





Wing

Span, ft	22.69
Area, sq ft	166.5
Aspect ratio	3.09
Taper ratio	0.39
Sweep, 0.25c, deg	15.9
Dihedral, deg	0
Over-all length, ft	66.75

Figure 11.- Two-view drawing and principal dimensions of airplane A.



Airplane A				F6F-3	
Symbol	hp	M	P	P	Symbol
○	3,000	0.30	3.4	3.7	○
		0.50	3.0	3.2	
		0.70	2.3	2.2	
□	35,000	0.60	3.4	3.3	□
		0.90	3.2	3.2	
		1.00	2.6	2.1	

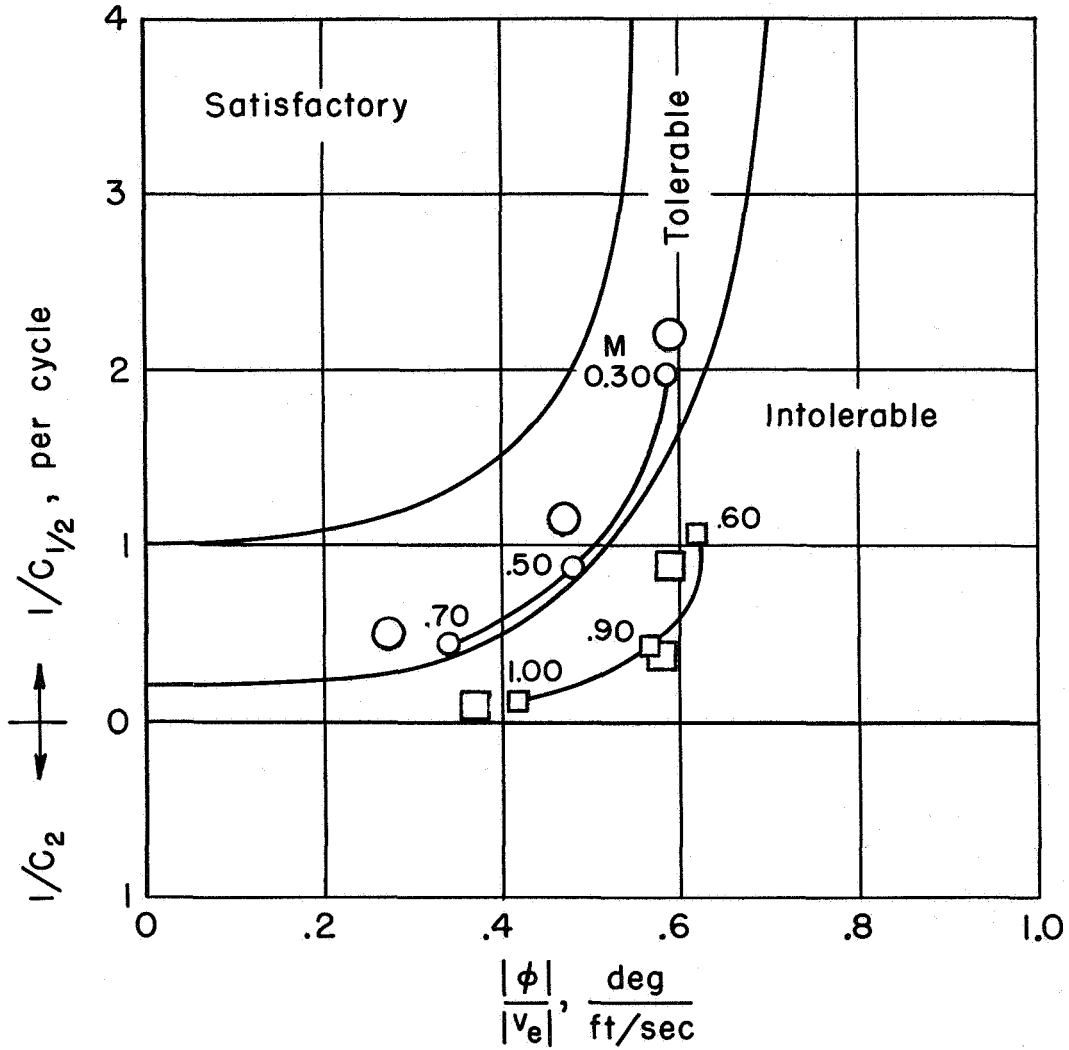
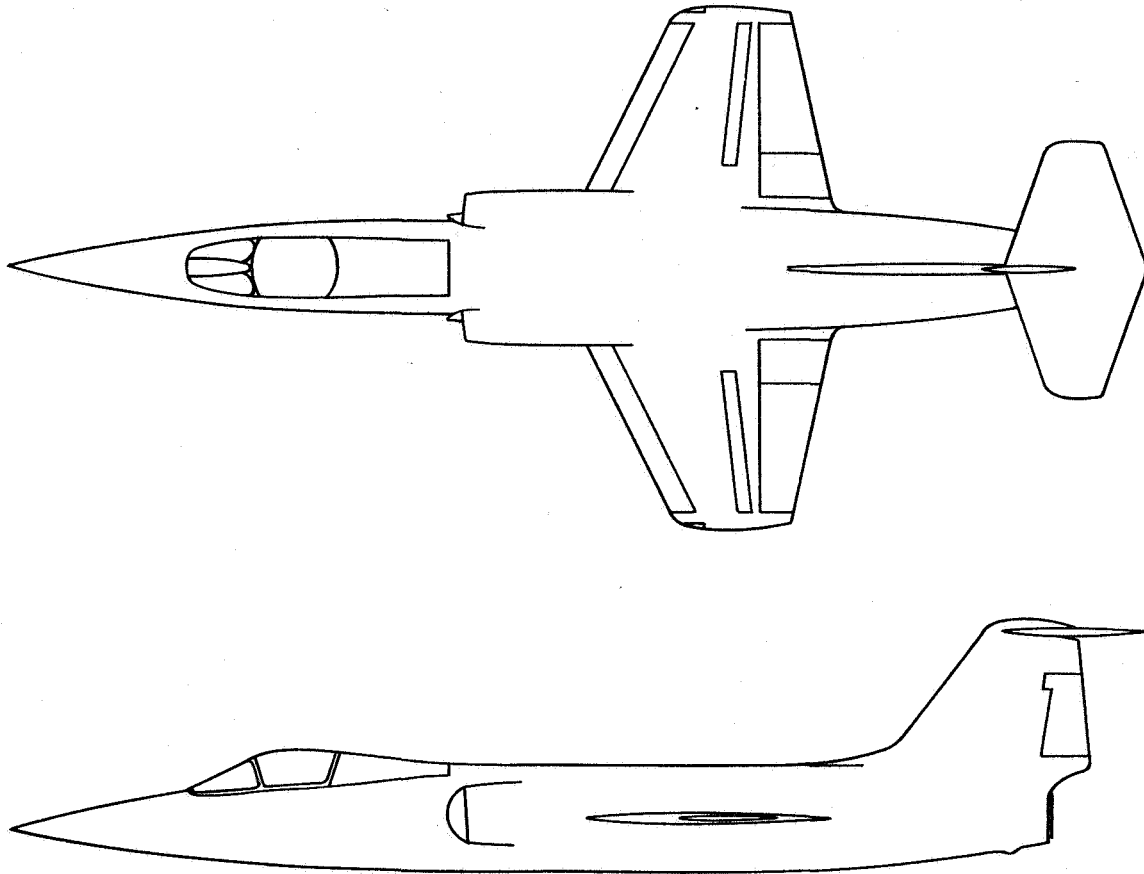


Figure 12.- Predicted lateral oscillatory characteristics of airplane A and measured lateral oscillatory characteristics of the variable-stability F6F-3 compared with the pilot-opinion boundaries of reference 2.





Wing		
Span, ft		22.08
Area, sq ft		191
Aspect ratio		2.5
Taper ratio		0.38
Sweep, 0.25c, deg		18
Dihedral, deg		0
Over-all length, ft		48.25

Figure 13.- Two-view drawing and principal dimensions of airplane B.

Airplane B				F6F-3		
hp	M	P	Condition	Symbol	P	Symbol
35,000	0.90	2.0	Design C_{nr}	○	2.2	⊙
			$3 \times$ Design C_{nr}	□	2.2	⊠
			$6 \times$ Design C_{nr}	◇	2.2	⊠
			$2 \times$ Design C_{nr}	△	2.3	△
Sea level	0.24	2.5	Landing Config.	□	---	---

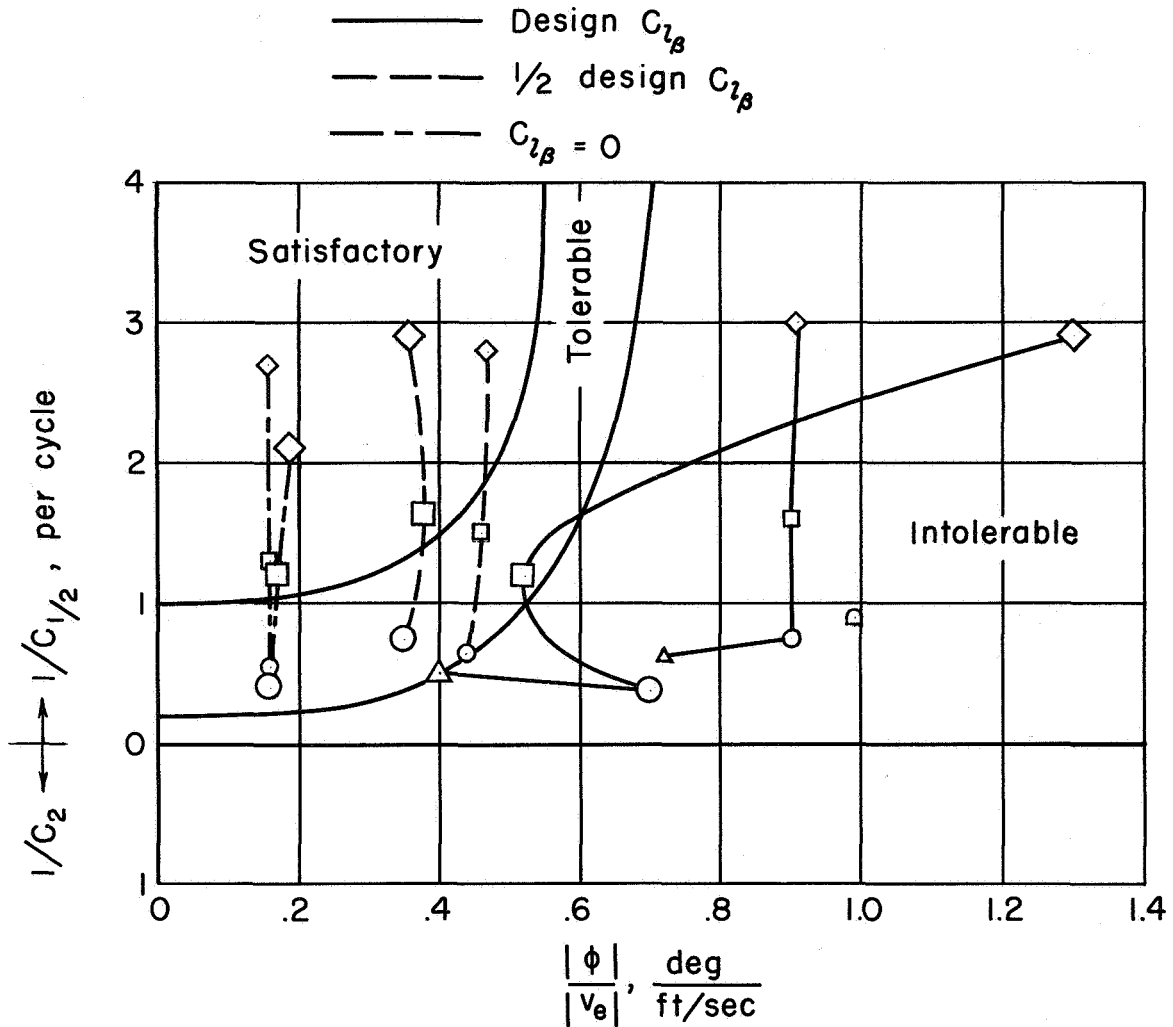


Figure 14.- Predicted lateral oscillatory characteristics of airplane B and measured lateral oscillatory characteristics of the variable-stability F6F-3 compared with the pilot-opinion boundaries of reference 2.

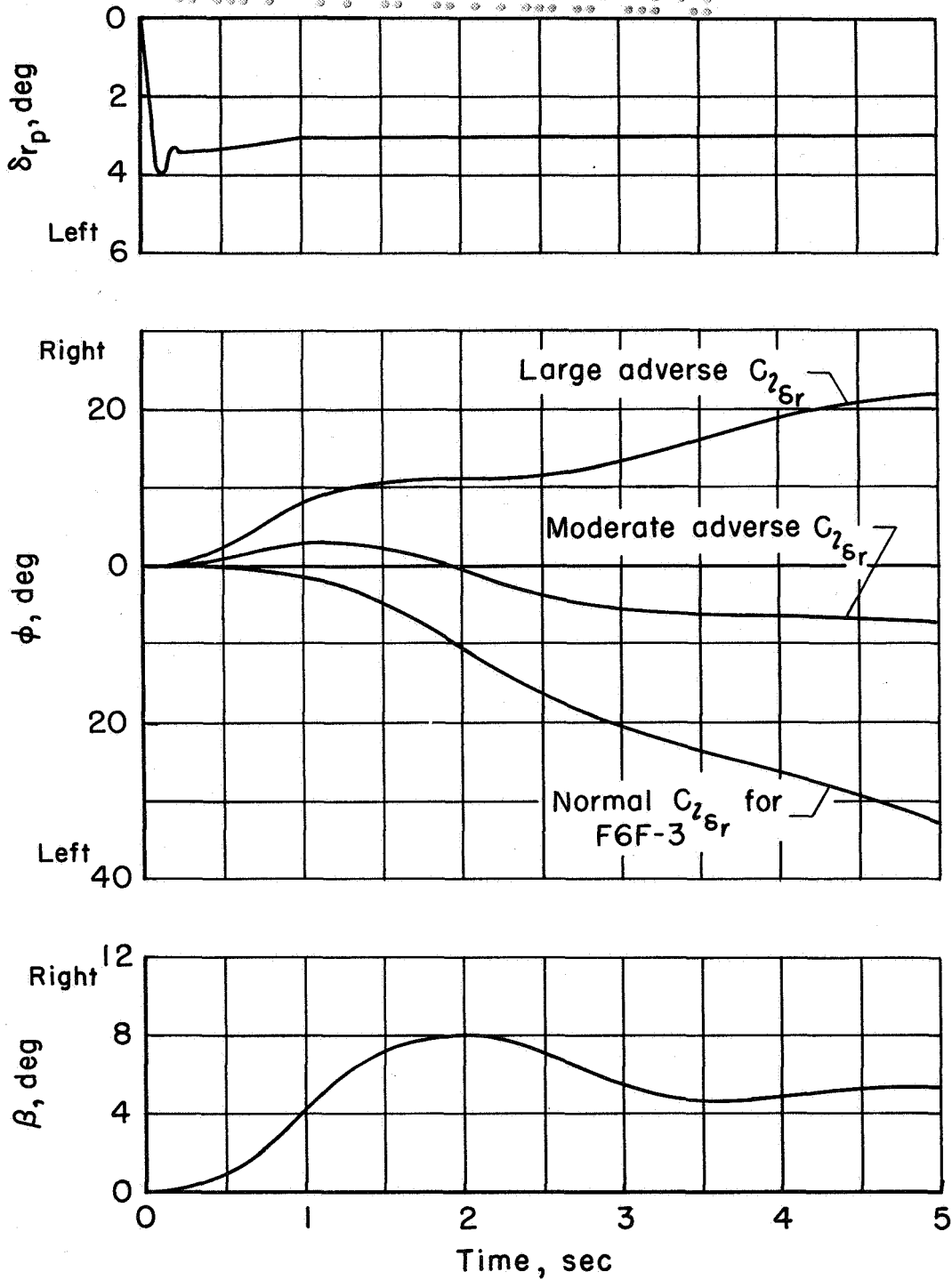
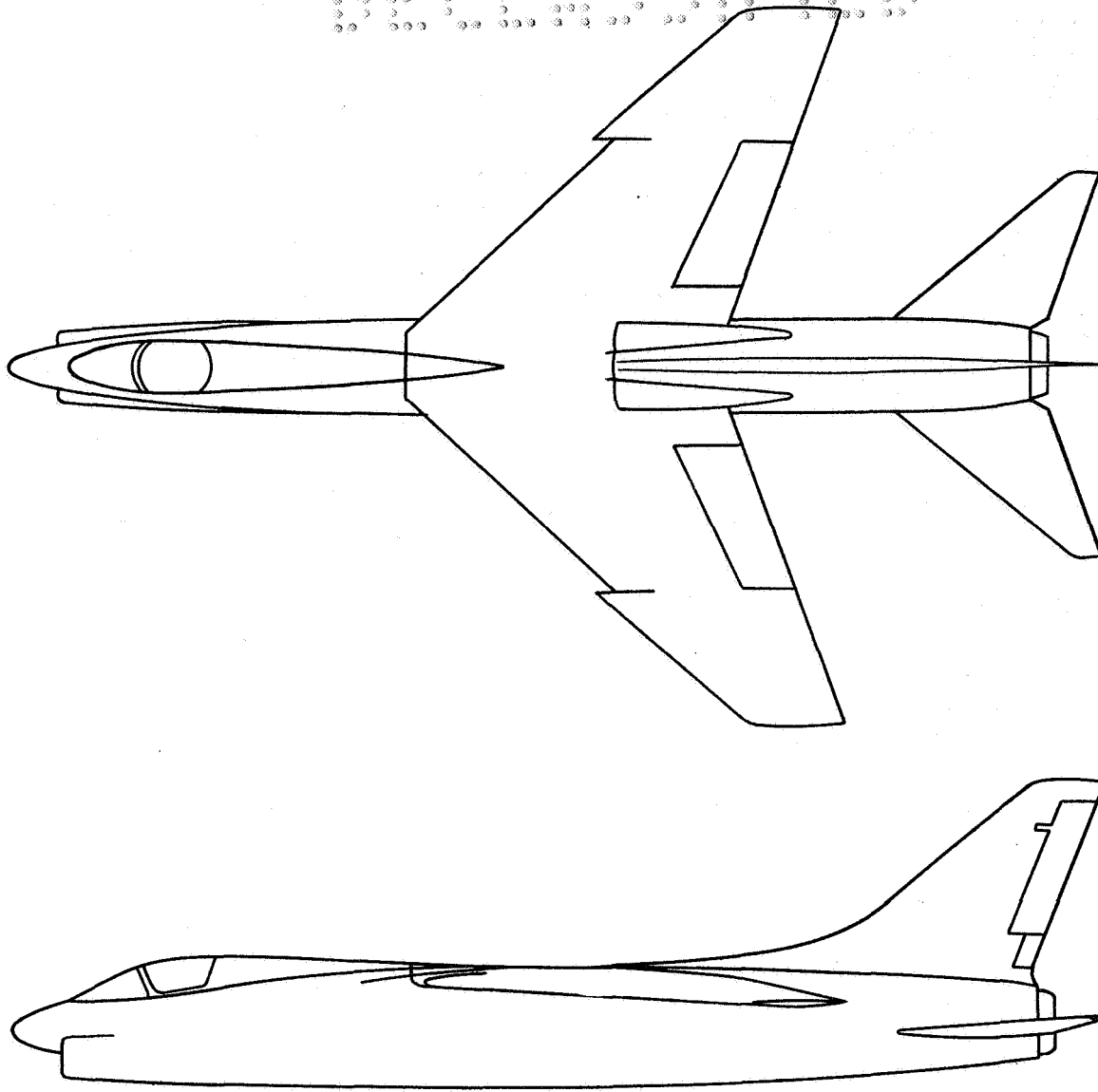


Figure 15.- Effect of $C_{l\delta_r}$ on roll response to abrupt rudder deflection for variable-stability F6F-3 airplane; one-half design $C_{l\beta}$ for airplane B.





Wing		
Span, ft		35.67
Area, sq ft		375.0
Aspect ratio		3.39
Taper ratio		0.25
Sweep, 0.25c, deg		42.0
Dihedral, deg		-5.0
Over-all length, ft		54.0

Figure 16.- Two-view drawing and principal dimensions of airplane C.



Airplane C				F6F-3		
h _p	V/V _{SL}	Symbol	Damper	P	P	Symbol
0	1.5	○	None	3.5	2.9	○
	1.2			3.5	3.0	
	1.2	□	Yaw	3.7	3.5	□
		◇	Roll	4.2	3.4	◇

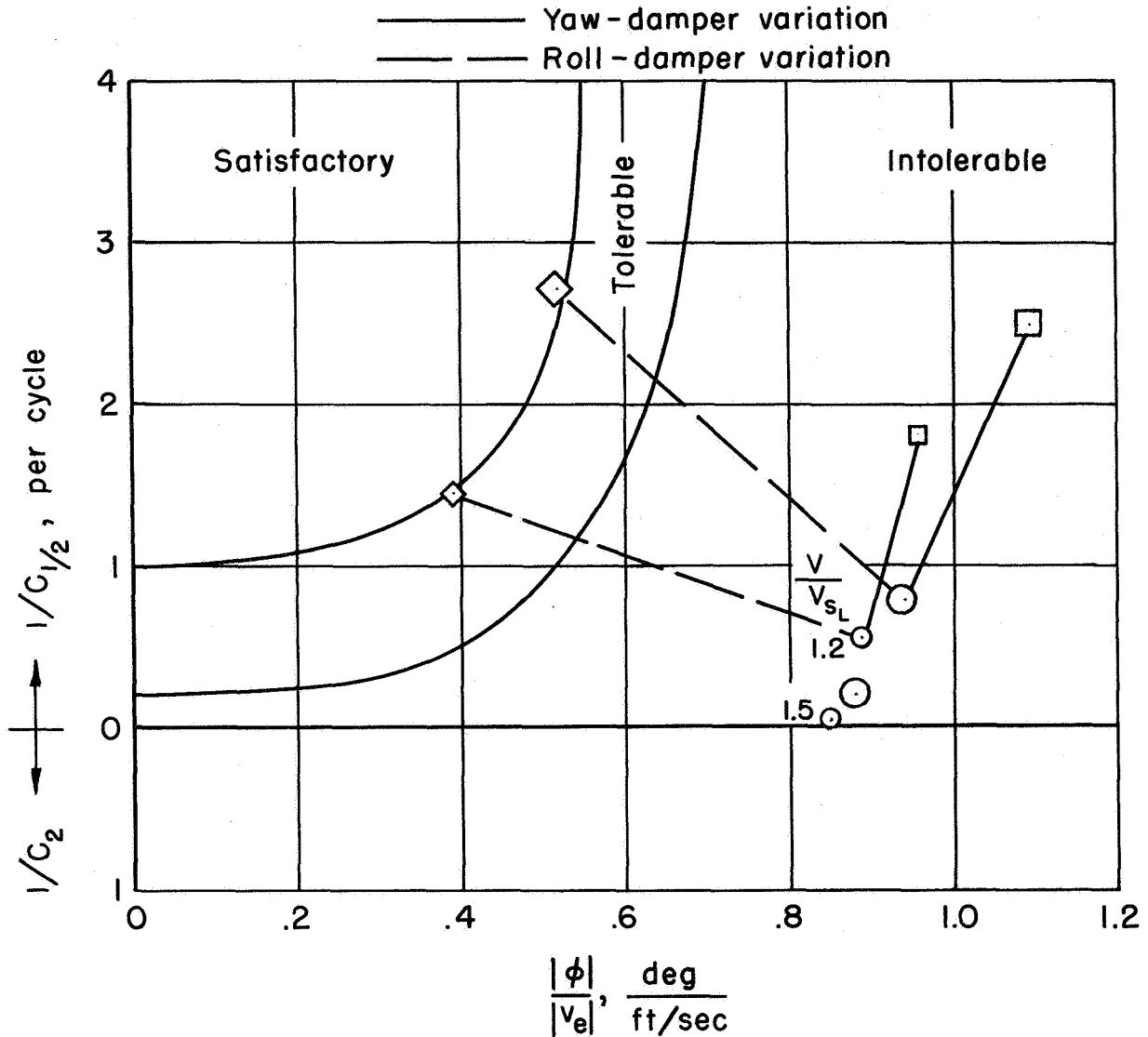


Figure 17.- Predicted lateral oscillatory characteristics of airplane C and measured lateral oscillatory characteristics of the variable-stability F6F-3 compared with the pilot-opinion boundaries of reference 2.



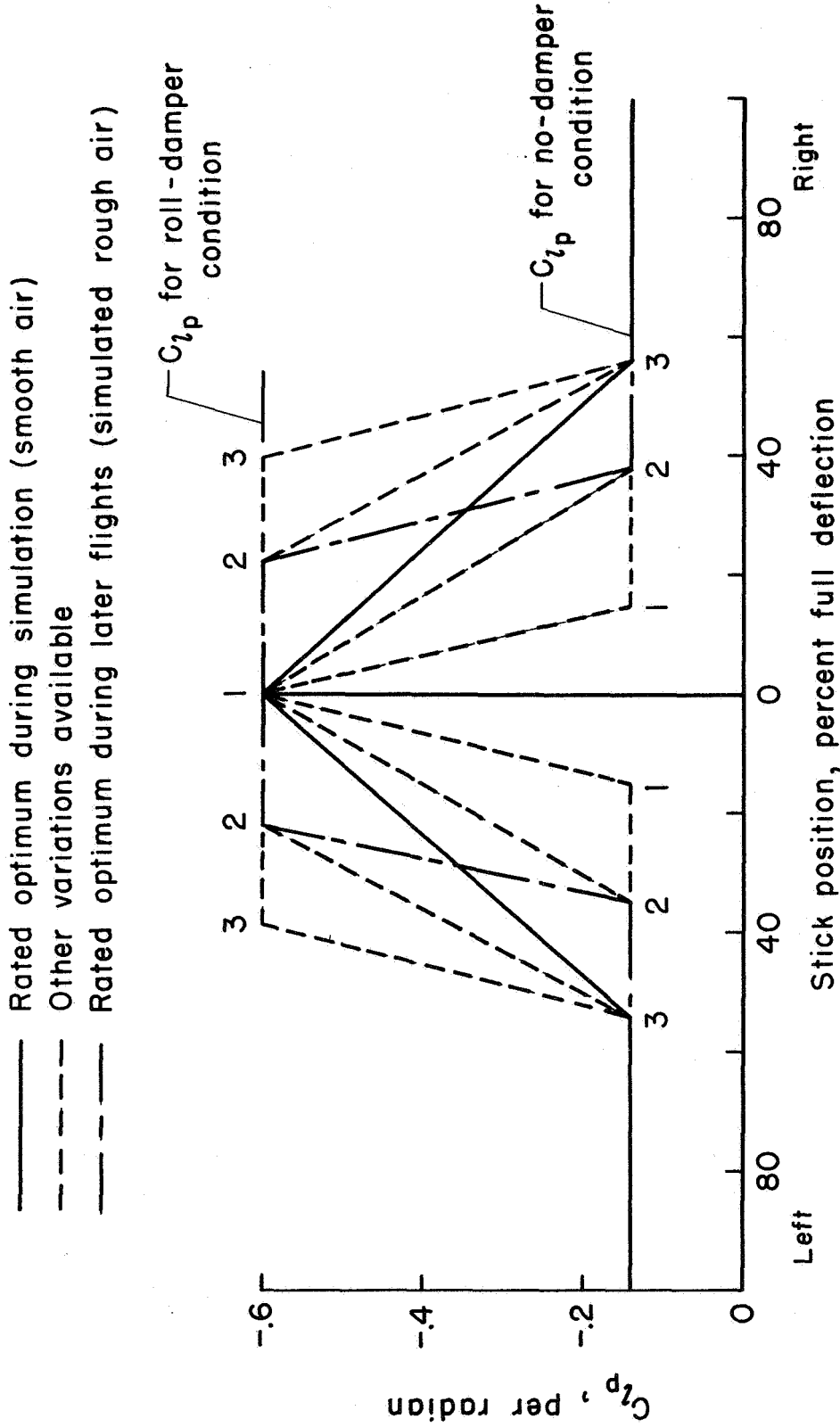
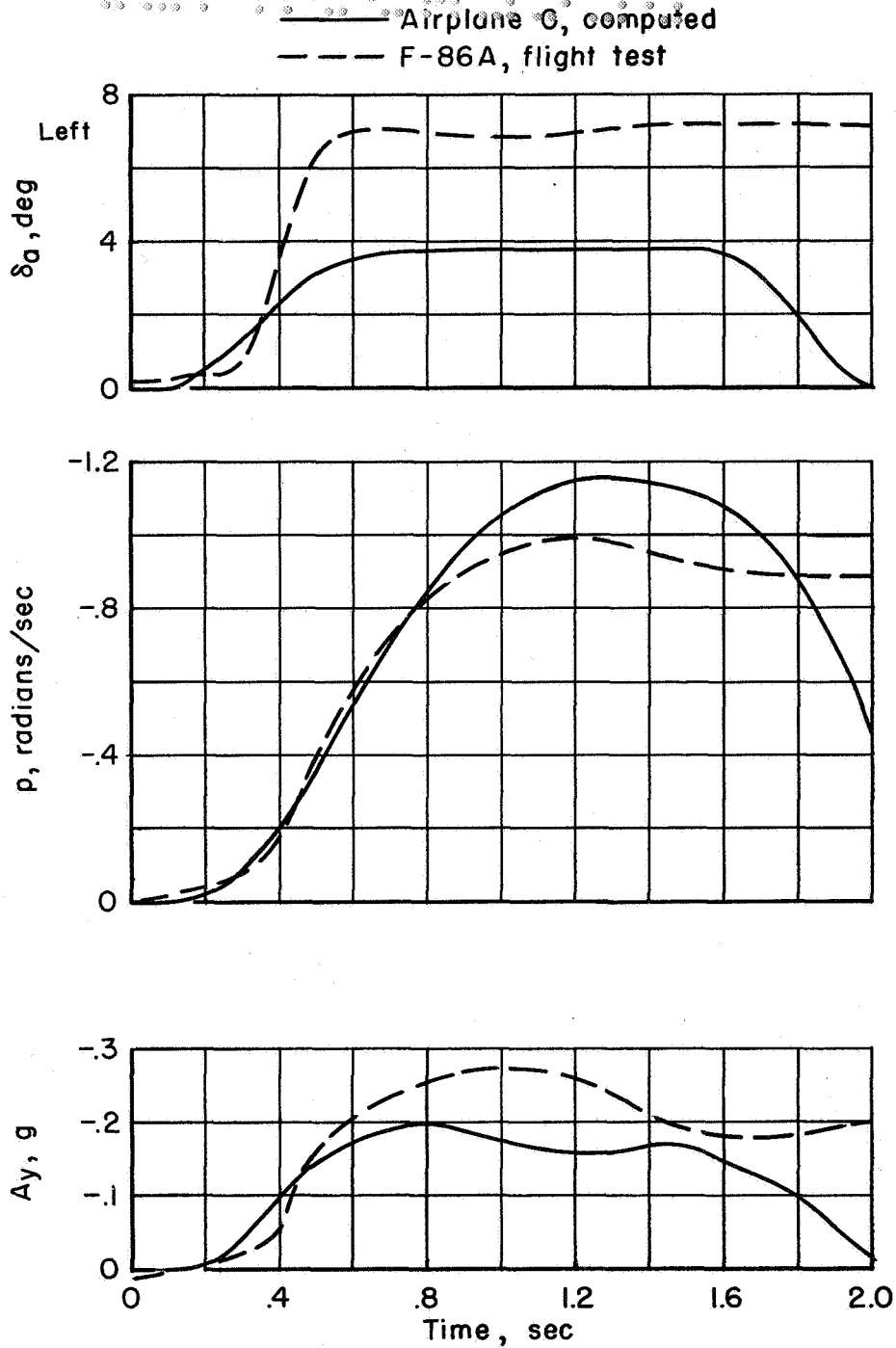
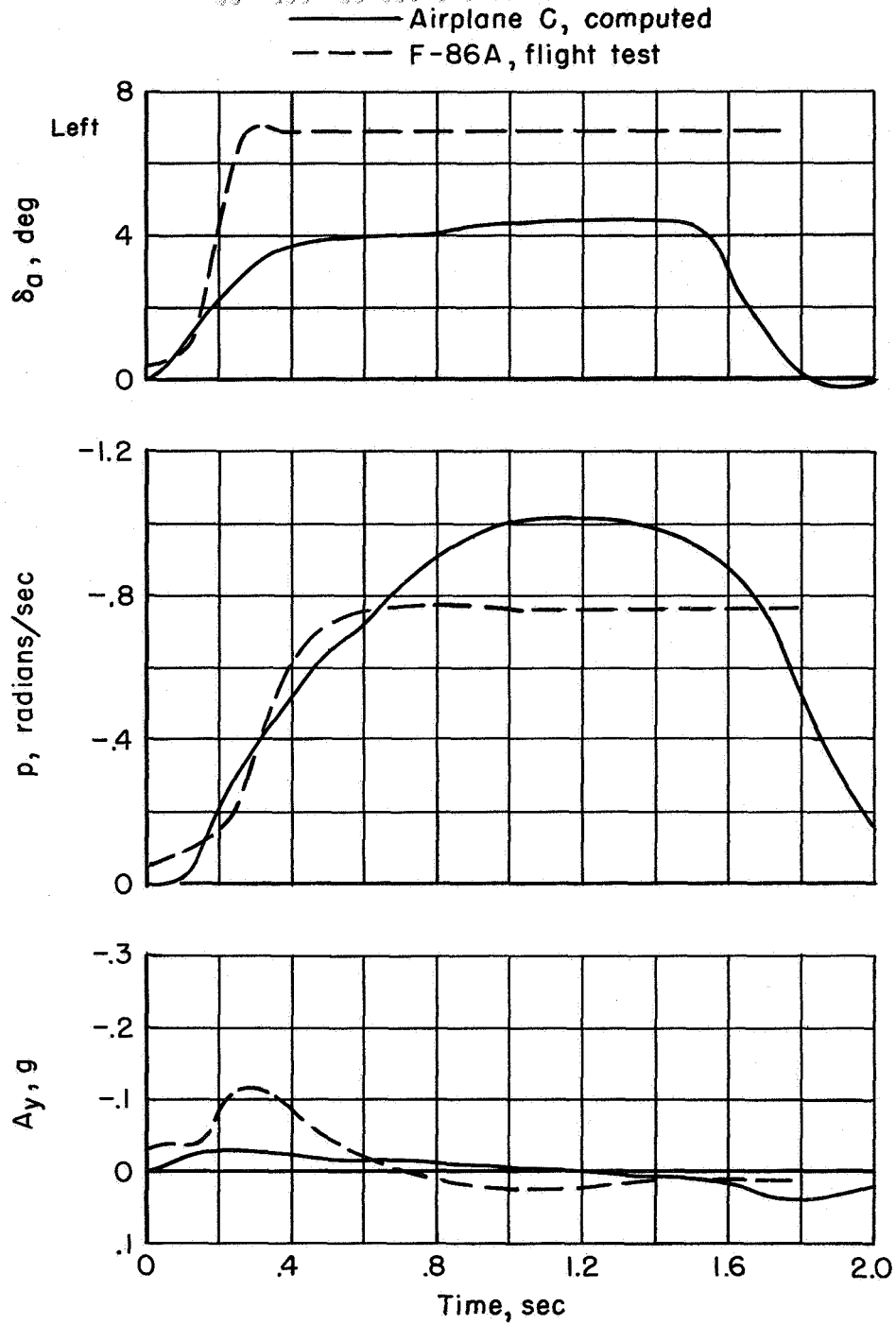


Figure 18.- Six variations of C_{lp} with lateral stick position made available in the variable-stability F6F-3 airplane.



(a) Basic condition (no aileron-rudder interconnection).

Figure 19.- Rolling-velocity and lateral-acceleration responses to abrupt pedals-fixed aileron deflections computed for airplane C, compared with measured responses of the variable-stability F-86A.

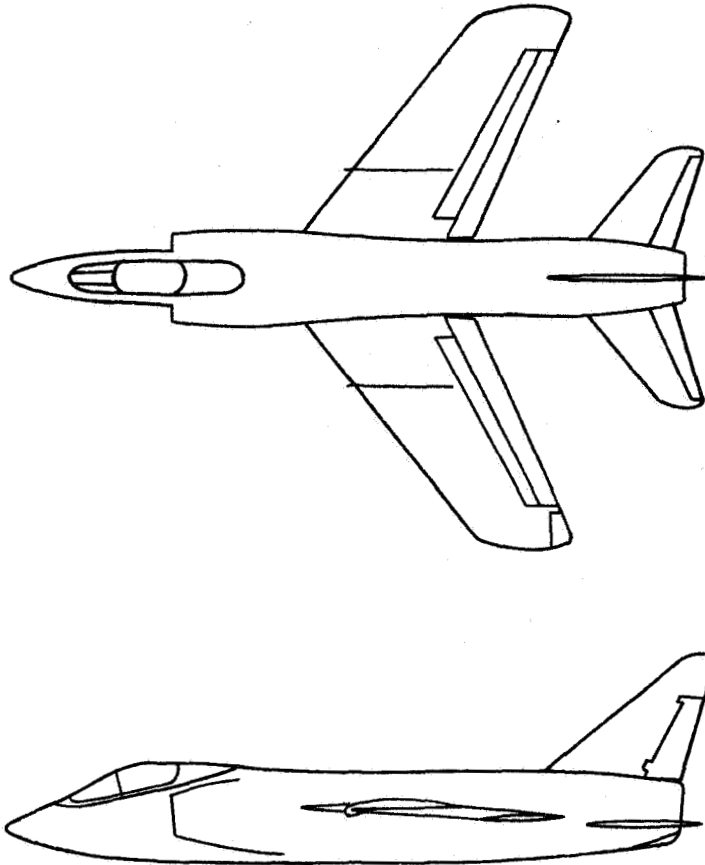


(b) Improved condition (with aileron-rudder interconnection).

Figure 19.- Concluded.

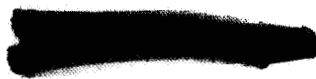


CONFIDENTIAL



Wing		
Span, ft		31.65
Area, sq ft		250.0
Aspect ratio		4.01
Taper ratio		0.50
Sweep, 0.25c, deg		35.0
Dihedral, deg		-2.5
Over-all length, ft		40.83

Figure 20.- Two-view drawing and principal dimensions of airplane D.



Airplane D						F6F-3	
Condition	hp	M	V/V _{SL}	Symbol	Average P	Average P	Symbol
Combat cruise	10,000	0.64	---	▽	1.8	2.3	□
	40,000	1.41	---	□	1.5		
	55,000	0.70	---	◇	3.1	2.8	○
Power approach	0	---	1.1	△	3.8		
		---	1.4	◇	3.4	3.0	◇
P/A, reduced C _{nβ}		---	1.1	◻	4.0	3.0	◻

Flagged symbols indicate yaw damper

- Yaw-damper variation
- Roll-damper variation

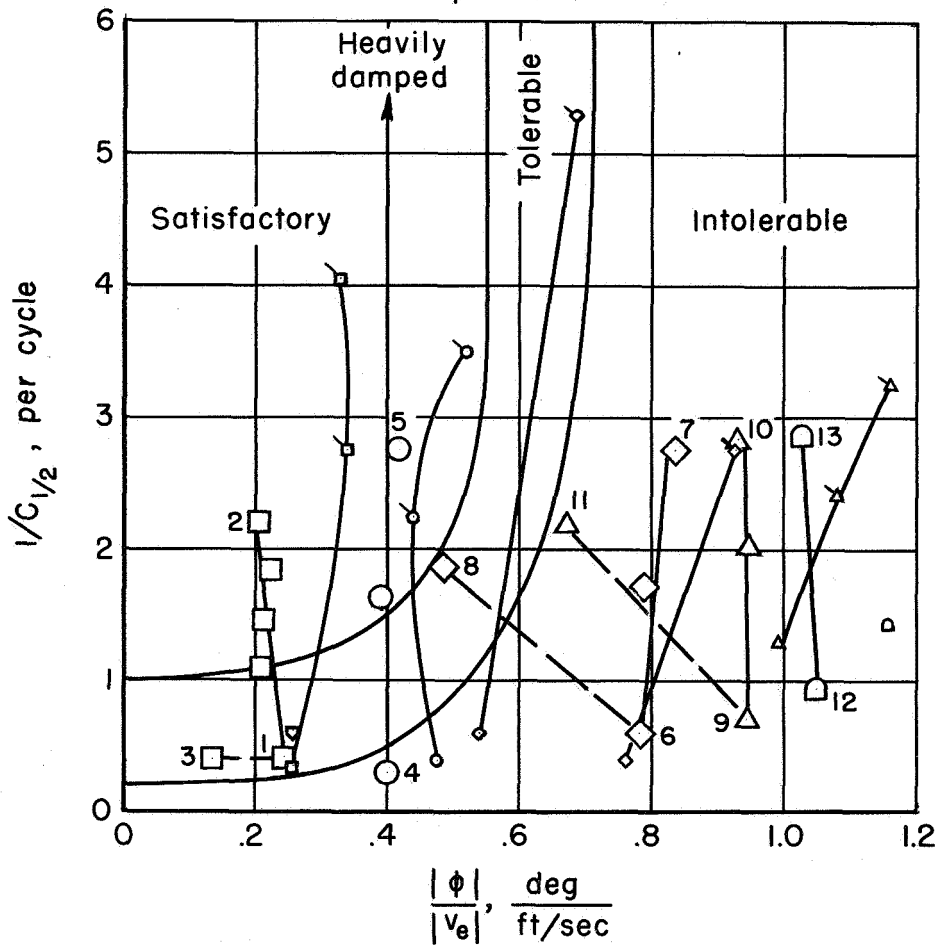


Figure 21.- Predicted lateral oscillatory characteristics of airplane D and measured lateral oscillatory characteristics of the variable-stability F6F-3 compared with pilot-opinion boundaries of reference 2.



Airplane D				F-86A	
hp	M	Symbol	P	P	Symbol
10,000	0.91	◊	1.1	1.0	◊
	1.15	○	0.9	1.5	○
40,000	1.41	◻	1.5	1.6	◻

Flagged symbol indicates yaw damper
 $(C_{nr}/C_{nr} = 11.74)$
 design

———— F-86A yaw-damper variation

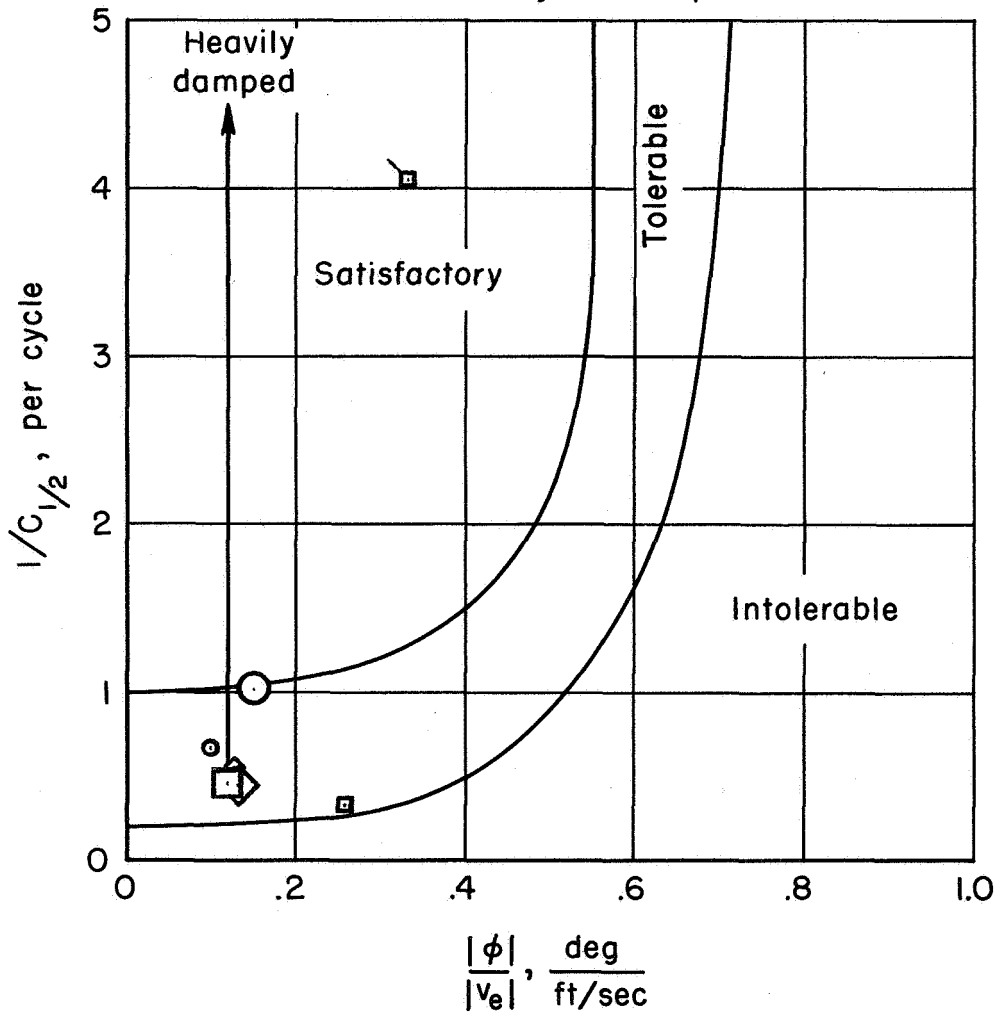
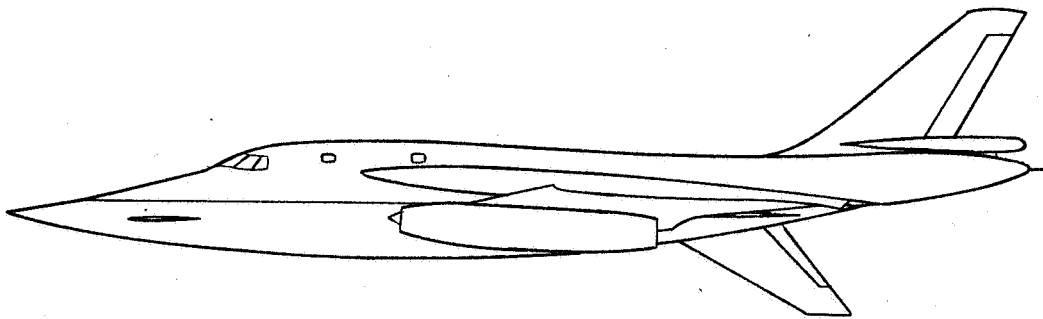
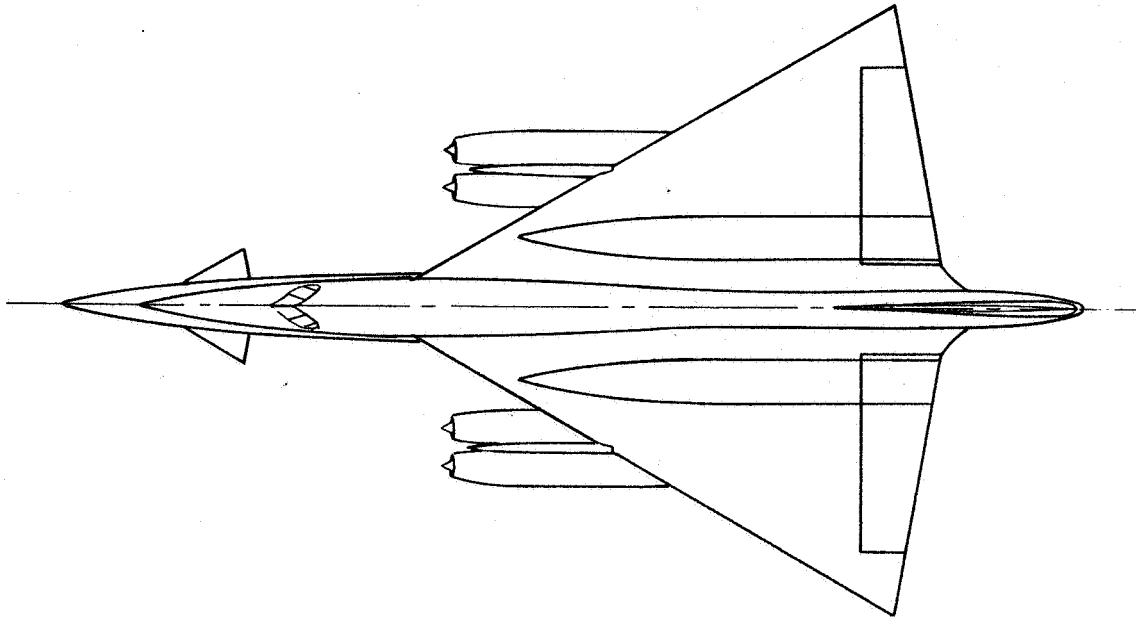


Figure 22.- Predicted lateral oscillatory characteristics of airplane D and measured lateral oscillatory characteristics of the variable-stability F-86A compared with pilot-opinion boundaries of reference 2; combat cruise condition.





Wing		
Span, ft	56.86	
Area, sq ft	1542.0	
Aspect ratio	2.096	
Taper ratio	0	
Sweep, 0.25c, deg	51.5	
Dihedral, deg	0	
Over-all length, ft	95.00	

Figure 23.- Two-view drawing and principal dimensions of airplane E as simulated by variable-stability F6F-3.



Airplane E					F6F-3	
Symbol	Condition	hp	M	P	P	Symbol
○	Take-off	0	0.35	4.6	3.4	○
□	Refuel	30,000	0.60	4.4	4.0	□
◇	High speed	---	---	5.7	5.7	◇
△	High speed	---	---	4.8	4.4	△
▴	High speed	---	---	4.8		

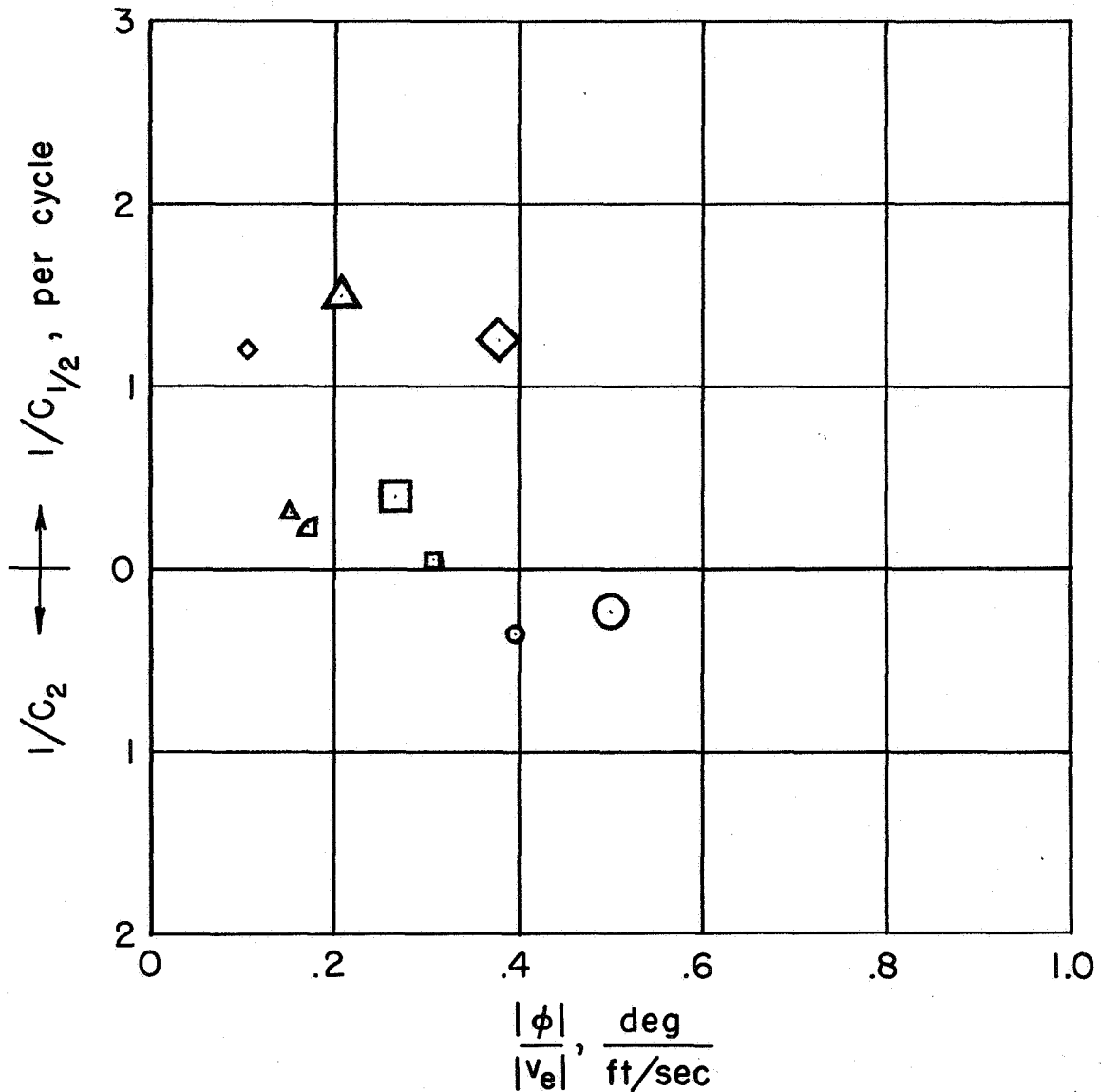
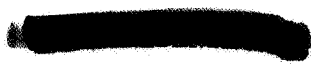


Figure 24.- Predicted lateral oscillatory characteristics of airplane E and measured lateral oscillatory characteristics of the variable-stability F6F-3.



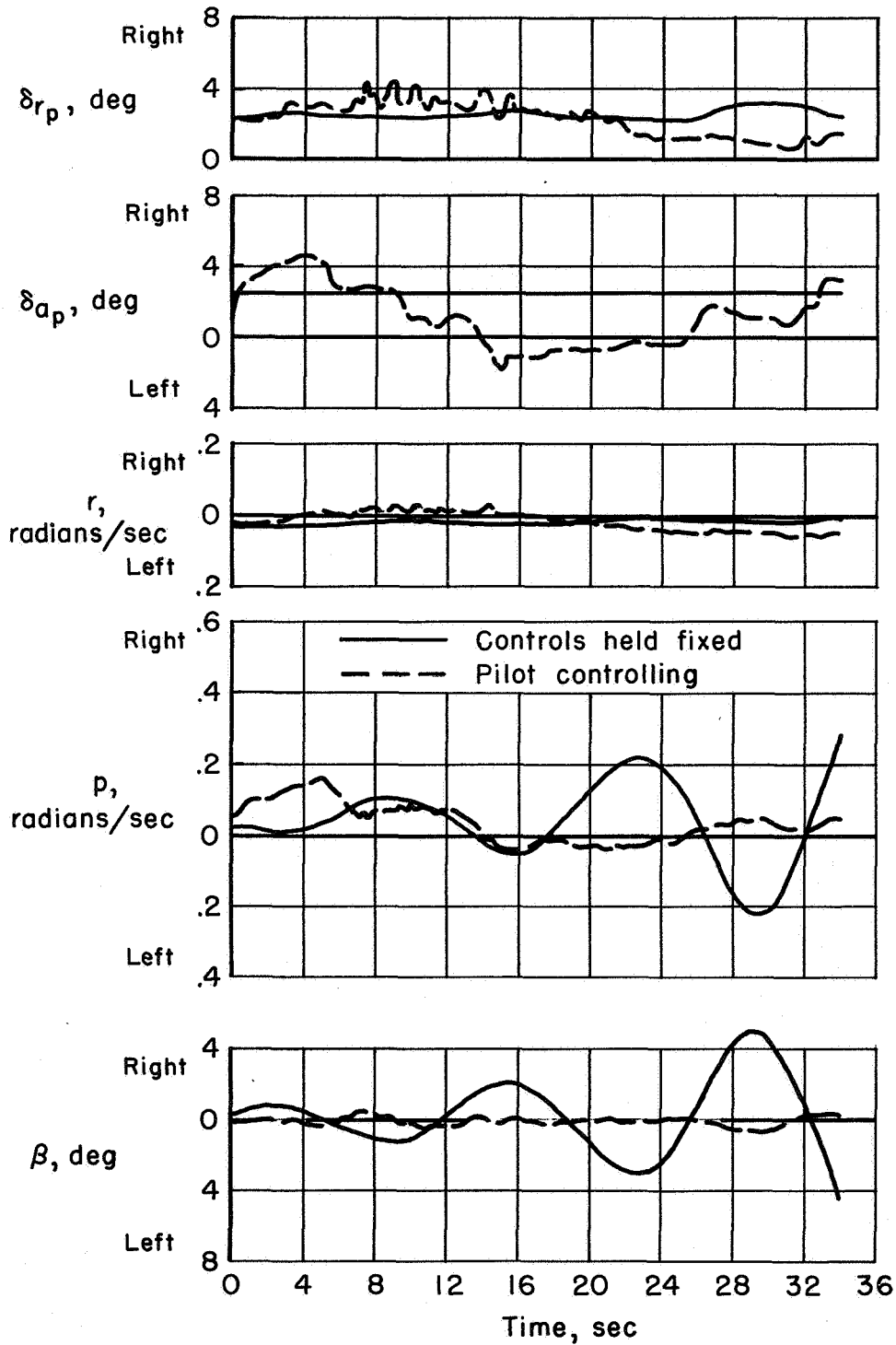
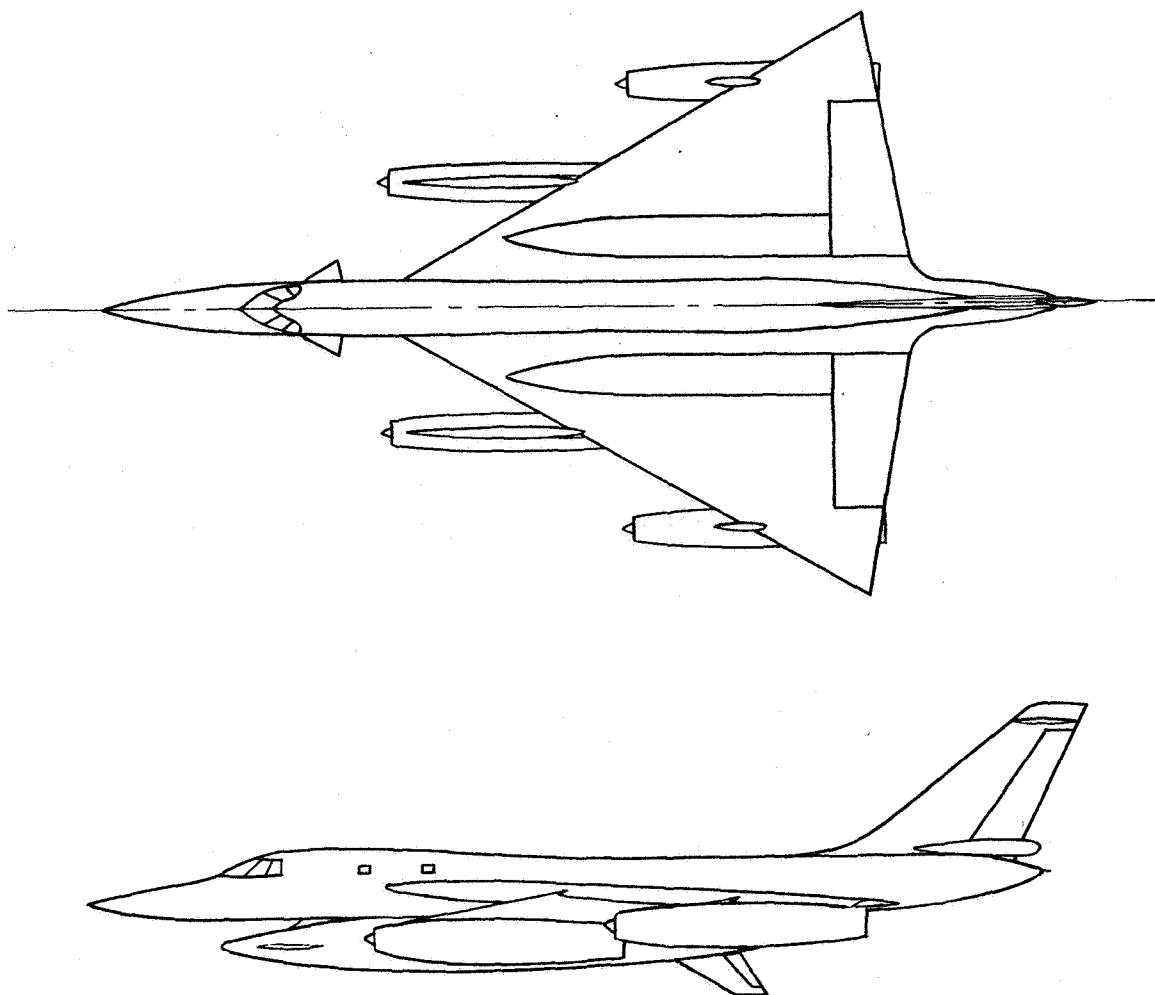


Figure 25.- Time histories of lateral and directional motions of the variable-stability F6F-3 with low directional stability; $C_{n\beta} \approx 0$.

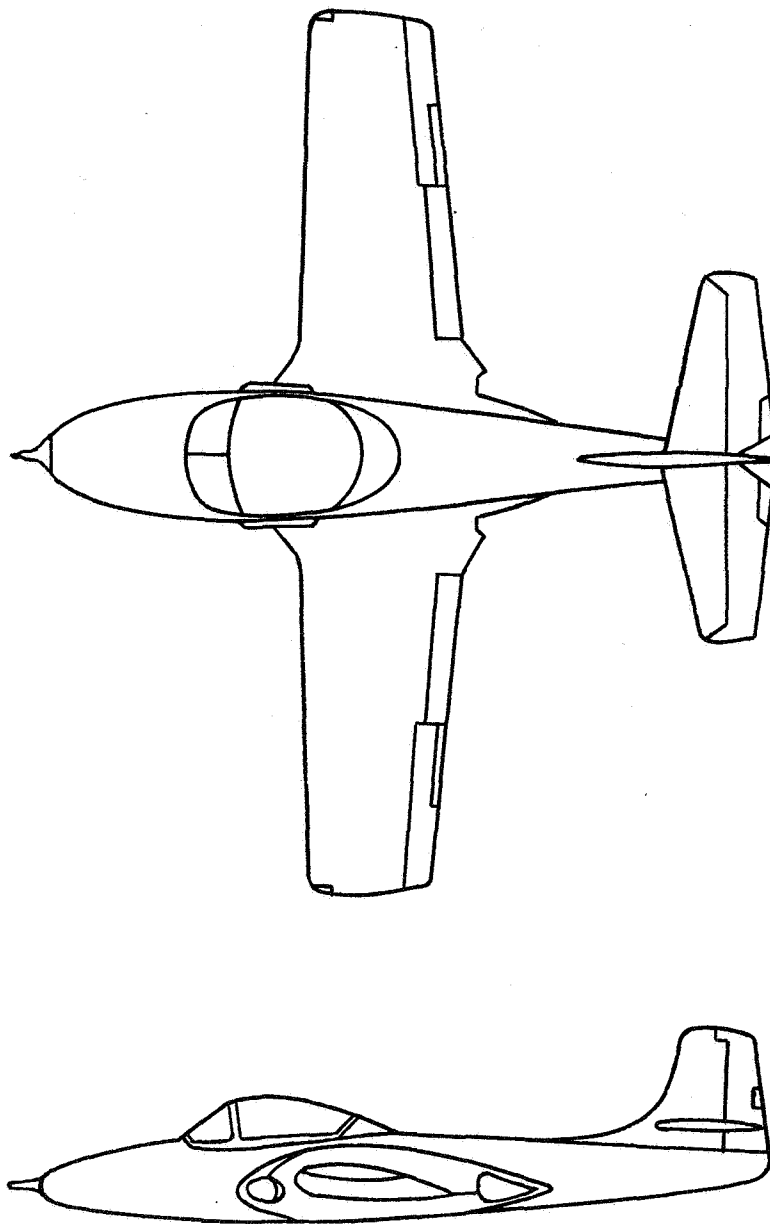




Wing		
Span, ft	56.86	
Area, sq ft	1542.0	
Aspect ratio	2.096	
Taper ratio	0	
Sweep, 0.25c, deg	51.5	
Dihedral, deg	2.23	
Over-all length, ft	96.78	

Figure 26.- Two-view drawing and principal dimensions of airplane E as simulated by variable-stability F-86A.





Wing		
Span, ft	33.0	
Area, sq ft	181.8	
Aspect ratio	6.0	
Taper ratio	0.64	
Sweep, 0.25c, deg	0	
Dihedral, deg	2	
Over-all length, ft	27.1	

Figure 27.- Two-view drawing and principal dimensions of airplane F.



Airplane F					F6F-3	
Symbol	Condition	hp	V, mph	P	P	Symbol
○	Climb	0	220	2.3	2.1	○
□	Landing	0	109	4.8	3.0	□

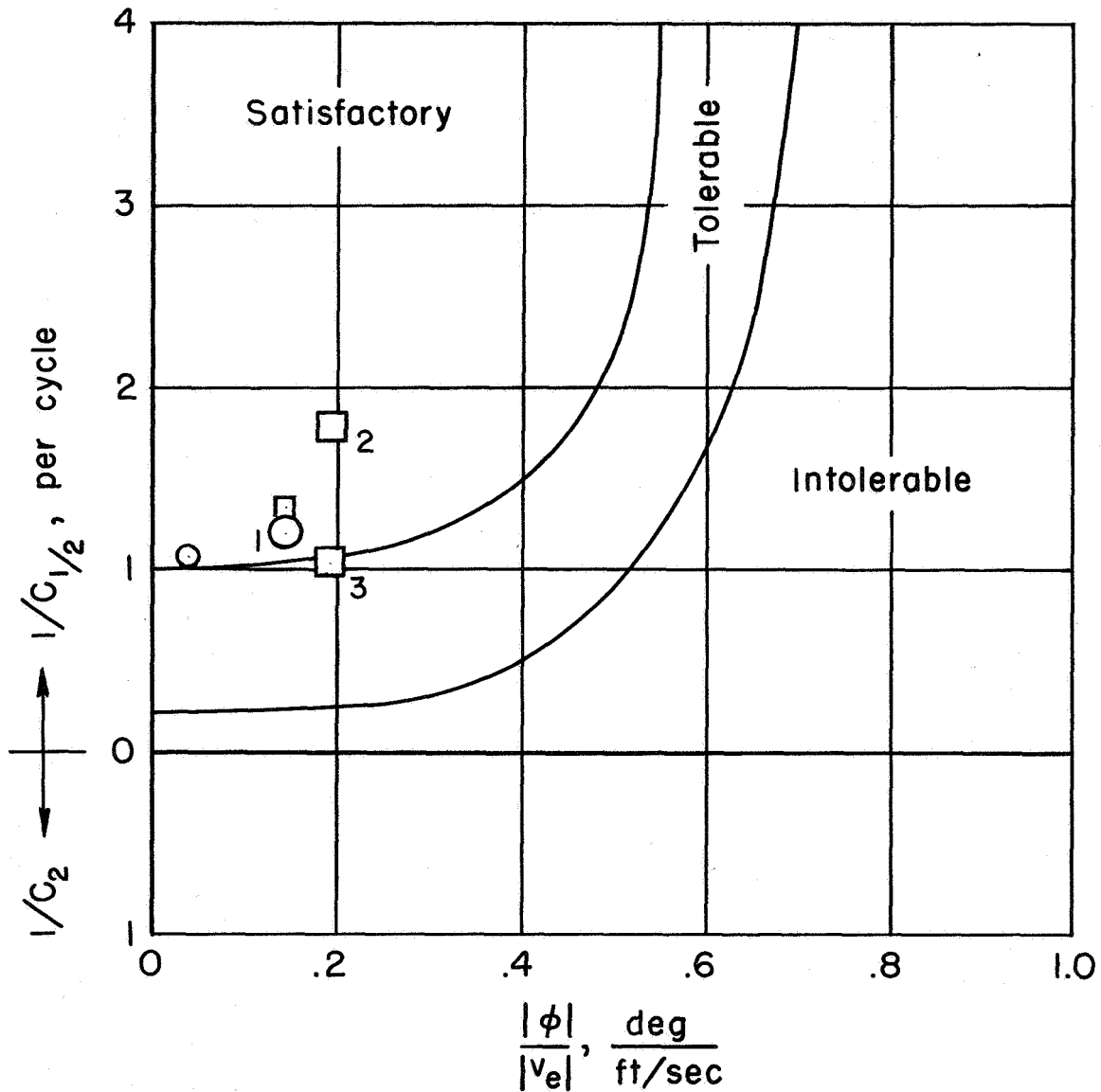


Figure 28.- Predicted lateral oscillatory characteristics of airplane F and measured lateral oscillatory characteristics of the variable-stability F6F-3 compared with the pilot-opinion boundaries of reference 2.



